MARTIN MARIETTA ENERGY SYSTEMS LIBRARIES

3 4456 0330557 2

ORNL/TM-11748

OAK RIDGE NATIONAL LABORATORY

MARTIN MARIETTA

Sensitivity Comparison of Intrinsic Germanium Detectors with Various Efficiencies

L. M. L. Buker

OAK RIDGE NATIONAL LABORATORY
CENTRAL RESEARCH LIBRARY
CIRCULATION SECTION
4500N ROOM 175
LIBRARY LOAN COPY
DO NOT TRANSFER TO ANOTHER PERSON
If you wish someone else to see this report, send in name with report and the library will arrange a loan.

MANAGED BY
MARTIN MARIETTA ENERGY SYSTEMS, INC.
FOR THE UNITED STATES
DEPARTMENT OF ENERGY

This report was prepared as an [illegible] of the United States Government. Neither the United States Government nor any agency thereof, nor any their employees, makes any warranty, express or implied, or assumes any legal liability or responsibility for the accuracy, completeness, or usefulness of any information, apparatus, product, or process disclosed, or represents that its use would not infringe privately owned rights. Reference herein to any specific commercial product, process, or service by trade name, trademark, manufacturer, or otherwise, does not necessarily constitute or imply its endorsement, recommendation, or favoring by the United States Government or any agency thereof. The views and opinions of authors expressed herein do not necessarily state or reflect those of the United States Government or any agency thereof.

ORNL/TM-11748

SENSITIVITY COMPARISON OF INTRINSIC GERMANIUM DETECTORS WITH VARIOUS EFFICIENCIES

A Thesis

Presented for the

Master of Science Degree

The University of Tennessee, Knoxville

Louise M. Love Buker

December 1990

Prepared by the
Oak Ridge National Laboratory
Oak Ridge, Tennessee 37831
managed by
Martin Marietta Energy Systems, Inc.
for the
U. S. DEPARTMENT OF ENERGY
under Contract No. DE-AC05-84OR21400

MARTIN MARIETTA ENERGY SYSTEMS LIBRARIES
3 4456 0330557 2

ACKNOWLEDGEMENTS

Dr. Laurence Miller of the University of Tennessee has assured continued technical support throughout the three plus years of this research study. Dr. Miller was instrumental in changing my career path and encouraging me to pursue a Masters Degree in Nuclear Engineering.

I wish to acknowledge EG&G ORTEC employees Dr. Ronald Keyser and Richard Seymour for their early discussions and support. Their discussions have proven invaluable to me. I also wish to thank Murf Trammell and EG&G ORTEC for providing me with an opportunity to utilize their low background counting facilities for the conduction of this work.

ABSTRACT

This study has acquired a large volume of empirical data for a wide range of relative efficiency germanium detectors. The purpose was to determine the sensitivity of various efficiency high-purity (P-type) germanium detectors produced by a single manufacturer. Selecting efficiency as the only variable and essentially all other variables remaining constant narrowed the field of detectors to 30. This investigation compares the response for the lower limit of detection (LLD), figure-of-merit (FOM), and minimum detectable activity (MDA) versus efficiency. In addition to the efficiency, the resolution, background, peak-to-Compton (P/C), and crystal shape of a p-type detector are of particular importance when considering the parameters of a detectors performance.

A concise summary of the results is that the detector of choice for low energy measurements would be a 25% detector with resolution better than 1.8 keV FWHM for the 1.332 keV energy of Co-60. The detector of choice for energy levels greater than 500 keV would be a high efficiency low background detector. If the entire energy range is of interest, then a 70% low background detector with a high P/C and a resolution better than 1.9 keV would yield the lowest MDA and assure the most efficient counting times.

TABLE OF CONTENTS

SECTION PAGE

1. INTRODUCTION 1
2. THEORY 7
3. EXPERIMENTAL 14
4. SPECTRUM ANALYSIS 21
   4.1 Implementation of Software Analysis Program . . 22
   4.2 Background Calculation 24
   4.3 Creating Nuclide Libraries 26
   4.4 Calibration 26
5. RESULTS 32
   5.1 Detection Efficiency 38
6. CONCLUSIONS 61
7. SUMMARY 65

REFERENCES 67

APPENDIXES
APPENDIX A. NUCLIDE AND LIBRARY TABLES 69
APPENDIX B. TABLES FOR FIGURES 75
   B.1 Raw Detector Data 76
   B.2 Figure Of Merit Data at 123 keV for Selected Detectors to Plot Figures 6 and 9 77
   B.3 Figure Of Merit Data at 1274.4 keV for Selected Detectors to Plot Figures 6 and 9 78
   B.4 Lower Limits of Detection at Background Peak Energies for Figures 7, 10, 11, and 12 79
   B.5 Calibration Spectra Minimum Detectable Activities at Non-Peak Energies (A-150) for Figures 13 and 16 80
   B.6 Background Spectra Minimum Detectable Activities at Non-Peak Energies (B-150) for Figures 14 and 17 81
   B.7 Background Spectra Minimum Detectable Activities at Peak Energies for Figure 15 . . . 82
   B.8 Background Spectra Lower Limit of Detection for Different Count Times at Peak Energies . 83
   B.9 Count Time versus Minimum Detectable Activity for Figures 20, 21, 22, 23, and 24 84
   B.10 Count Time versus Figure of Merit (1/MDA) for Figure 21 85
   B.11 Peak-to-Compton and Figure-of-Merit (FOM) Values to Plot Figure 25 86

VITA 87

LIST OF TABLES

TABLE PAGE

Appendix A
A.1 Low Background Nuclide List: Photopeak Energies for Isotopes of Interest in Low Background Studies . . .70
A.2 Certificate Table for Mixed Gamma Radionuclide Standard 71
A.3 Activities of Standard Reference Source 72
A.4 Calibration Library (4275B.LIB). Gamma-ray Energies, Emission Rates, and Half-life Data for SRM-4275b . . 72
A.5 Calibration Library List for Minimum Detectable Activity Analysis of SRM 4275b, Filename (4275.LIB), for Peak and Non-Peak Regions of Interest 73
A.6 Background Library List for Peak (Pks-100) and on-Peak (B-150) Regions of Interest for Nuclide Energies, Emission Rates and Half-life 74

LIST OF FIGURES

FIGURE PAGE

1. Cutaway View of Germanium Detector Cryostat 4
2. Picture of Lead Shield 16
3. Simple Energy Spectroscopy System 18
4. Programs and Disk Files of B30. 23
5. Energy-Efficiency Curve 29
6. Figure of Merit (FOM) versus Detector Efficiency . . 34
7. LLD versus Efficiency 35
8. Peak-to-Compton versus Energy 37
9. FOM versus Efficiency 41
10. Comparison of LLD for Standard and LB Detectors . . . 42
11. LLD versus Energy for Similar Resolution 44
12. Comparison of LLD for Standard (56%) and LB Detectors 45
13. MDA versus Energy for Calibration Spectra 46
14. MDA versus Efficiency for Background Spectra 48
15. MDA versus Efficiency for Background Peaks 49
16. MDA versus Efficiency for Calibration Spectra 50
17. MDA versus Energy for Background Spectra 51
18. MDA and LLD Comparison 53
19. Count Time versus LLD 54
20. Count Time versus MDA for Different Energies 55
21. Count Time versus FOM 57
22. Count Time versus MDA for Different Eff. at 220 keV . 58
23. Count Time versus MDA for Different Eff. at 700 keV . 59
24. Count Time versus MDA for Different Eff. at 2300 keV 60
25. Comparison of Peak to Compton and FOM 63

LIST OF SYMBOLS

Symbol	Definition
A_m	Reciprocal of the fractional error
b	Channels/keV in the peak
B	Background
$B_{c2}(E_1)$	Compton background interference at energy $(E)_1$, from gamma-ray E_2 at higher energy
B_n (E_1)	Natural background interference at gamma ray one
D_m	Minimum detectable disintegration rate
ϵ	Absolute photopeak efficiency
E_1	Energy one
$\epsilon_{c2}(E_1)$	Compton efficiency for gamma ray two
FOM	Figure-of-Merit
$F_2(E_1)$	FOM for detecting gamma one in the presence of gamma two
Γ	Gammas per decay for the photopeak
KTA	Kerntechnischer Ausschuss, KTA-1503.1, (Nuclear Technical Studies)
LLD	Lower Limit of Detection
MDA	Minimum Detectable Activity
N_m	Peak counts detectable after background subtracted
R	Resolution
ROI	Region-of-Interest
σ	Standard deviation of the background
t	Live-time of counting interval

1. INTRODUCTION

Scientists today are being asked to measure concentrations of radionuclides at increasingly lower levels. This creates a demand for better resolution detectors with larger efficiencies that can provide the necessary sensitivity to accurately determine low levels of radioactivity. This study quantitatively determines the appropriate detector for a particular measurement based upon background measurements of various efficiency high purity germanium detectors. There are predominately two different cases affecting the selection process. The first case is when a radiation source emits high energy photons that significantly contribute to the Compton continuum. The second case is when the nuclides being analyzed emit photons that are similar in energy to the background radiation of the detector cryostat. This also results in a loss of sensitivity.

[The sensitivity of a gamma-ray detector is defined by Cooper as a measure of its ability to detect a gamma-ray peak in the presence of interference from natural radioactivity and Compton scattering of higher energy gamma rays originating in the source.][1]

Various levels of sensitivity are obtained by choice of detector and measurement time. For very low levels of

activity and a standard germanium detector of 20% efficiency (relative to a 3" x 3" NaI) it might be necessary to count for a million seconds, or about 11.5 days. There are several reasons for the extremely long count time. First, the detectors have a relatively small efficiency. Second, the naturally occurring background of the environment degrades the lower limit of detection and third, the detector's natural background may add to the Compton continuum.[2]

The contributions to ambient background from external sources are varied in origin. These sources may be from cosmic rays, particle energies beyond the energies being measured, electronic noise, radon build-up inside the shield and Pb X-rays. These sources of background can be minimized by the appropriate selection of equipment, such as the use of a low background graded Z (atomic number) shield and to self-vent the shield with nitrogen gas to reduce the radon levels.

Source related background contributions are generally due to the natural radioisotopes contained in the materials of construction of a germanium detector. These originate from K-40, natural primordial emitters of uranium, thorium and their decay products, and man-made radionuclides such as Cs-137 and Co-60.[2] These sources are therefore an area over which the detector manufacturer has some control and is where the experimenter must make the most appropriate decision in

selecting a detector for the necessary measurements. In general the materials of construction for a detector are classified into three general categories:

1. Miscellaneous materials used in small quantities and not close to the crystal, such as O-rings and screws.
2. Large quantities of materials that are not in close proximity to the germanium crystal, such as the stainless steel flange. These materials are selected from preferred vendors who have provided samples for testing the radionuclide content. They have established a reliable track record for maintaining these low levels.
3. Large quantities of materials that are found in close proximity to the sensitive germanium crystal. All batches of these materials are measured before being utilized. This would include stainless steel screws, copper detector cups, beryllium entrance windows, lead back shields and magnesium end caps, to name a few of the items that can be found in close proximity to the detector crystal. Please see Figure 1 for a cutaway view of a germanium detector showing the various parts and their relationship to the crystal.

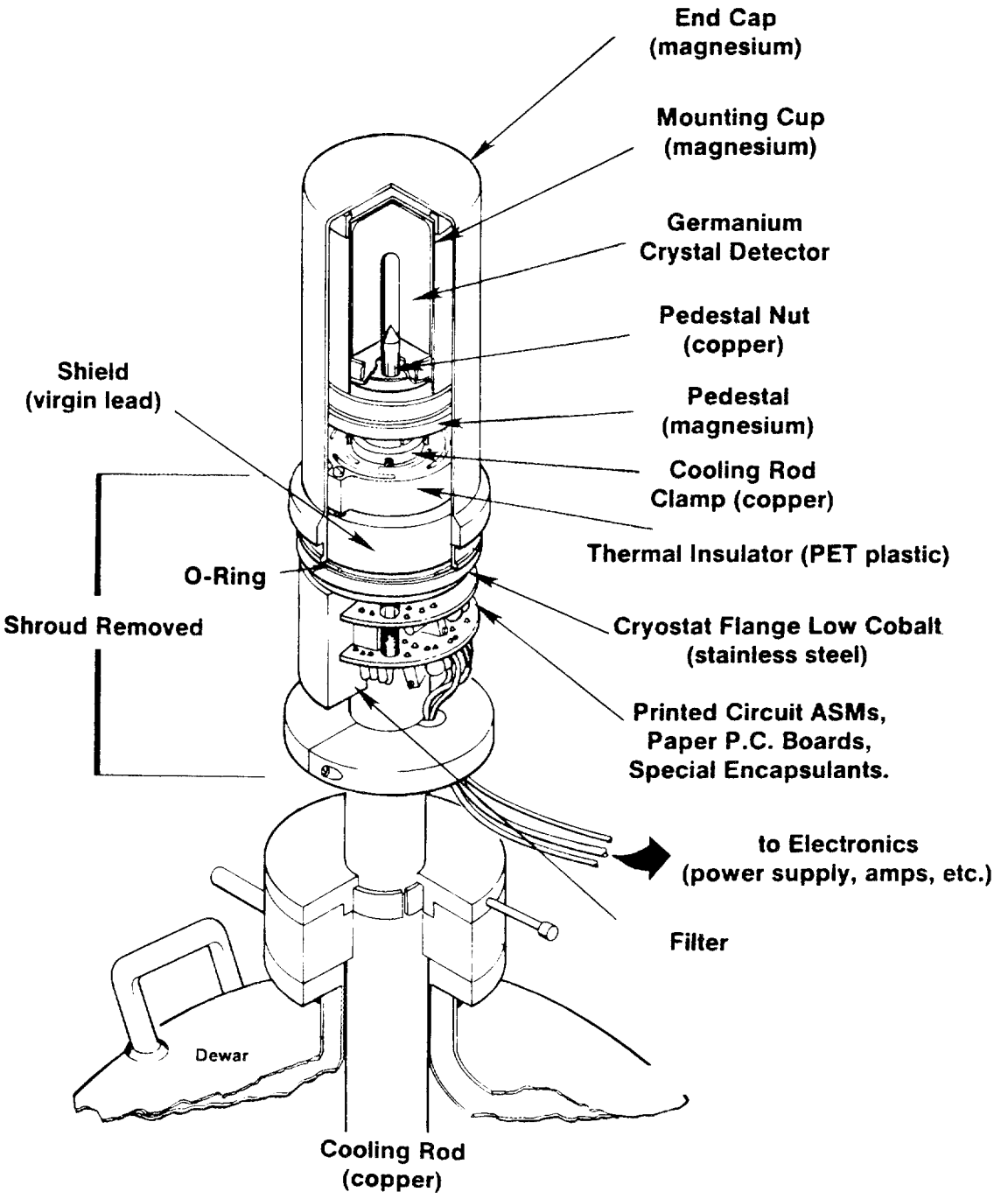

Fig. 1 Cutaway View of Germanium Detector Cryostat

Where extremely low levels of activity are concerned, the limiting factors for material selection are the following: those inherent in the detector used, the conditions under which the samples are measured, and the sophistication with which the results of the measurements are analyzed.

The determination of the relative sensitivity of various efficiency, high purity (p-type) germanium detectors is the purpose of this study. The background spectra are analyzed for their lower limits of detection (LLD) and for their relative minimum detectable activities (MDA) to show the relationship between increasing efficiency and decreasing LLD and MDA.[4] The calibration spectra are analyzed for relative MDA and figure of merit (FOM) to determine the relative sensitivity and counting uncertainty for source related sensitivity comparisons. The relative MDA values are analyzed for both peak and non-peak areas of the spectrum versus energy for various different efficiency detectors. Additionally, a few low background detectors are included to show a comparison of the increased sensitivity at several different efficiencies.

The relative MDA versus energy plots for different efficiency detectors show that a maximum difference for MDA's is reached at an energy ~750 keV. This means that for energies from ~600 to ~900 keV the gain in sensitivity for a

higher efficiency detector is more than would be normally expected. This study shows the energy ranges of radionuclide measurements where the use of a single larger efficiency detector has the most benefit in terms of sensitivity. This information will be of particular interest to those measuring environmental levels of radionuclides.

2. THEORY

A comparative analysis of the detection capability of various efficiency p-type detectors is based upon the lower limits of the measurement process. This lower limit is referred to as the "Lower Limit of Detection" (LLD).[5]

This limit depends upon a critical level of activity which is defined as the smallest count which indicates activity has been measured. This value also incorporates the statistical risk or probability of concluding falsely that sample activity is present.[6] The standard deviation of two sigma corresponds to the 95% confidence level for the two types of error. The first type of error is when there is no activity, and the second type is failing to detect activity, when in fact, there is activity. The LLD for the background spectrum at the 95% confidence level is defined by Pasternack and Harley[7] as,

$$LLD = 2*1.645*2^{\frac{1}{2}} * S \qquad (1)$$

where, S is the standard deviation of the background.

$$S = (B)^{\frac{1}{2}}/t \qquad (2)$$

The standard deviation of the distribution is the square root of the mean for a particular region of interest and the counting time is assumed to have no associated measurement error at low count rates.

Therefore the LLD for the background spectrum calculation at each photopeak energy of interest uses the following equation,

$$LLD = 4.66*(B)^{\frac{1}{2}}/(t * \epsilon * \Gamma) \quad (3)$$

where, B = gross counts in region of interest,

t = live-time of counting

ϵ = absolute photopeak efficiency, and

Γ = gammas per decay for the photopeak.

This equation indicates that the LLD is directly proportional to the square root of the background counts and inversely proportional to the livetime, efficiency, and gammas per decay. Therefore, increasing the counting time results in an improvement of the gamma spectroscopic measurement sensitivity. An increase in the counting time sufficient enough to realize an increase in the sensitivity is often not practical for a counting lab which measures many samples. This equation also shows that in order to increase sensitivity, a detector made with low background materials will lower the background and improve the sensitivity.

Another way to increase the sensitivity is to use detectors with larger relative efficiencies. An increase in efficiency increases the signal to noise ratio, also known as the peak-to-Compton measurement. However, larger volume detectors generally have slightly degraded resolutions as

compared to smaller efficiency detectors. The combination of these two factors alters the results away from an inversely linear relationship after a certain efficiency level of about 80% is reached. This will be explained in further detail in Chapter 5 of this paper.

The sensitivity of a gamma spectrometer is a measure of its ability to detect a gamma peak in the presence of interferences due to both Compton scattering and natural radioactivity. From first principles, the minimum detectable disintegration rate D(m) is an inverse measure of the analytical sensitivity and is given by the following equation:[3]

$$D_m = N_m \ / \ \epsilon * \Gamma * t \qquad (4)$$

where: N_m = peak counts detectable after background subtraction,

ϵ = detector efficiency for gamma ray of interest,

Γ = gamma emission rate for energy of interest, and

t = counting interval or live-time

Further development of the above equation for statistical variance of the measured peak in the presence of multiple gamma-rays yields the "minimum" detectable disintegration rate at E_1 as follows:[1]

$$D_m(E_1) = \frac{A_m\{[2bR(E_1)[B_{c2}(E_1)+B_n(E_1)] + A^2{}_m/4]^{\frac{1}{2}} + A_m/2\}}{\epsilon(E_1)\ \Gamma} \qquad (5)$$

A_m = reciprocal of the fractional error,[1]

b = channels/keV (the reciprocal of the gain, which when multiplied by the resolution gives the number of channels in the peak),

$R(E_1)$ = resolution at energy E_1,

$B_{c2}(E_1)$ = Compton background interference at energy $(E)_1$, from gamma-ray E_2 at a higher energy,

$B_n(E_1)$ = natural background interference at gamma-ray one,

$\epsilon(E_1)$ = peak efficiency for detecting gamma-rays of energy E_1,

Γ = fraction of disintegrations of the source for this gamma-ray energy, and

t = measurement interval.

This equation is based upon the assumption that if more than one gamma-ray contributes to the Compton interference, then $B_{C2}(E_1)$ is the sum of the individual contributions.

The two cases that predominate in this sensitivity calculation are the source induced background (Case 1) and the external background (Case 2). For the case where the $B_{C2}(E_1)$ is much greater than the natural background, the Compton interference will dominate the background term in Equation 5. This is because the resolution value and Compton

interference term are much larger than the A_m term. The sensitivity depends mainly on

$$D_m = \frac{[R(E_1)\ B_{c2}(E_1)]^{\frac{1}{2}}}{\epsilon(E_1)} \tag{6}$$

for the same A_m, b and t values. If it is assumed that the Compton background at gamma-ray one is constant for a given source geometry and a particular gamma-ray two, then the Compton efficiency for gamma-ray two ($\epsilon_{c2}(E_1)$) is also the same. Cooper proposed substituting this efficiency into the above equation and taking the reciprocal yielding the Figure-of-Merit (FOM) as

$$F_2(E_1) = \frac{\epsilon(E_1)}{[R(E_1)\,\epsilon_{c2}(E_1)]^{\frac{1}{2}}} \tag{7}$$

where, $F_2(E_1)$ is the detector FOM for detecting gamma ray one in the presence of gamma ray two. The detector with the largest FOM will have the highest sensitivity for detecting gamma-rays of energy E_1 in the presence of higher energy gammas.

The FOM is applied to the analysis of the calibration measurements because it accounts for detecting one gamma ray in the presence of one or more higher-energy nuclides. The FOM should give the best comparison for this study because the FOM is proportional to the efficiency and inversely proportional to the square root of the resolution and Compton efficiency. This will tend to normalize the calculation

results for the degraded resolution that is usually seen with higher efficiency detectors. The fact that the Compton efficiency is in the denominator means that reducing the Compton efficiency will give an improved FOM and increasing the peak-to-Compton (P/C) ratios will give an improved FOM.

For the second case (low background levels), Equation 5 is not rigorously applicable in absolute terms because the Poisson distribution does not then approximate a Gaussian distribution.[1] As recommended by Cooper the FOM should still be useful for the relative comparison of low-level systems if the total background term is considered in addition to the Compton interference. The LLD calculation (as given by Equation 1 and by the D_m calculation in Equation 5) incorporates the gross background counts into the derived MDA equation in the Spectrum Analysis Section.

The LLD versus relative efficiency curves give an inversely linear relationship of LLD with efficiency. A deviation from a strictly linear correlation exists for the larger relative efficiency detectors due to the larger volume of the crystal and materials in close proximity to the crystal. Larger volume detectors made with standard materials respond to both the source and background radiation simultaneously. Therefore, a comparison of low background detectors with standard detectors shows a relatively lower

level of detection by roughly a factor of two. This also will be shown later in the Results Section.

Another important comparison is to determine the effect of resolution upon the LLD values and to examine the MDA values for various efficiency detectors. The MDA's are based on non-peak and peak areas of the background spectrum, and they incorporate a normalization factor for resolution that the LLD values overlook. An evaluation of these two methods of analysis for similar efficiency detectors provides important information regarding the effect of resolution and efficiency on LLD values.

3. EXPERIMENTAL

The elimination of various parameters affecting the external background is accomplished through selection of data from the same low background cave and the same geometric configuration detector. The only variable is the efficiency and the associated measurement changes including the resolution and the peak-to-Compton values. The low background detectors are also of the same configuration with similar type of materials. All these detectors are calibrated for ~ 3600 seconds and the background measured for 100,000 seconds.

This selection process narrowed the total number of detectors included in the comparison to 30. Some of these detectors are very close in efficiency, allowing for a range of measured values and for a comparative analysis of the data. The following list outlines the criteria chosen to acquire a representative sampling:

1. High-purity germanium detector, transplantable on vertical configuration cyrostat. This eliminated the horizontal, and the side-looking configuration.
2. Lead shield, constructed of a two-inch thick oxygen free high conductivity copper liner, surrounded by a minimum of six inches of low background lead bricks supported with low background steel.

3. Amplifier, bias supply and ADC used were dedicated to the experiment to keep comparisons of selection criteria as consistent as possible.
4. A two point calibration software system for analyzing the spectrum. Also, a basic gamma-ray spectrum analysis software program for energy-efficiency calibrations and calculation of MDA values were used on all the data.
5. A National Institute of Standards and Technology (NIST) traceable mixed Europium-Antimony source measured at 10 centimeters from the endcap.

Tests were performed in the Low-Background Counting Laboratory at EG&G ORTEC, Oak Ridge, TN. The laboratory is located on the first level of a two-story brick building, at an altitude of approximately 1000 feet. A laboratory at sea level or below the ground will experience lower background measurements. This laboratory did have the added shielding afforded by being partially underground on the side of the building where the measurements were performed. However, the lead shield described above, in item two had shielding capabilities closer to a three pi configuration, rather than the much preferred four pi configuration. Figure 2 shows the outside design of the shield. The four inches of lead blocks on the floor prevented some of the radioisotopes from the building foundation and earth from reaching the counting system.

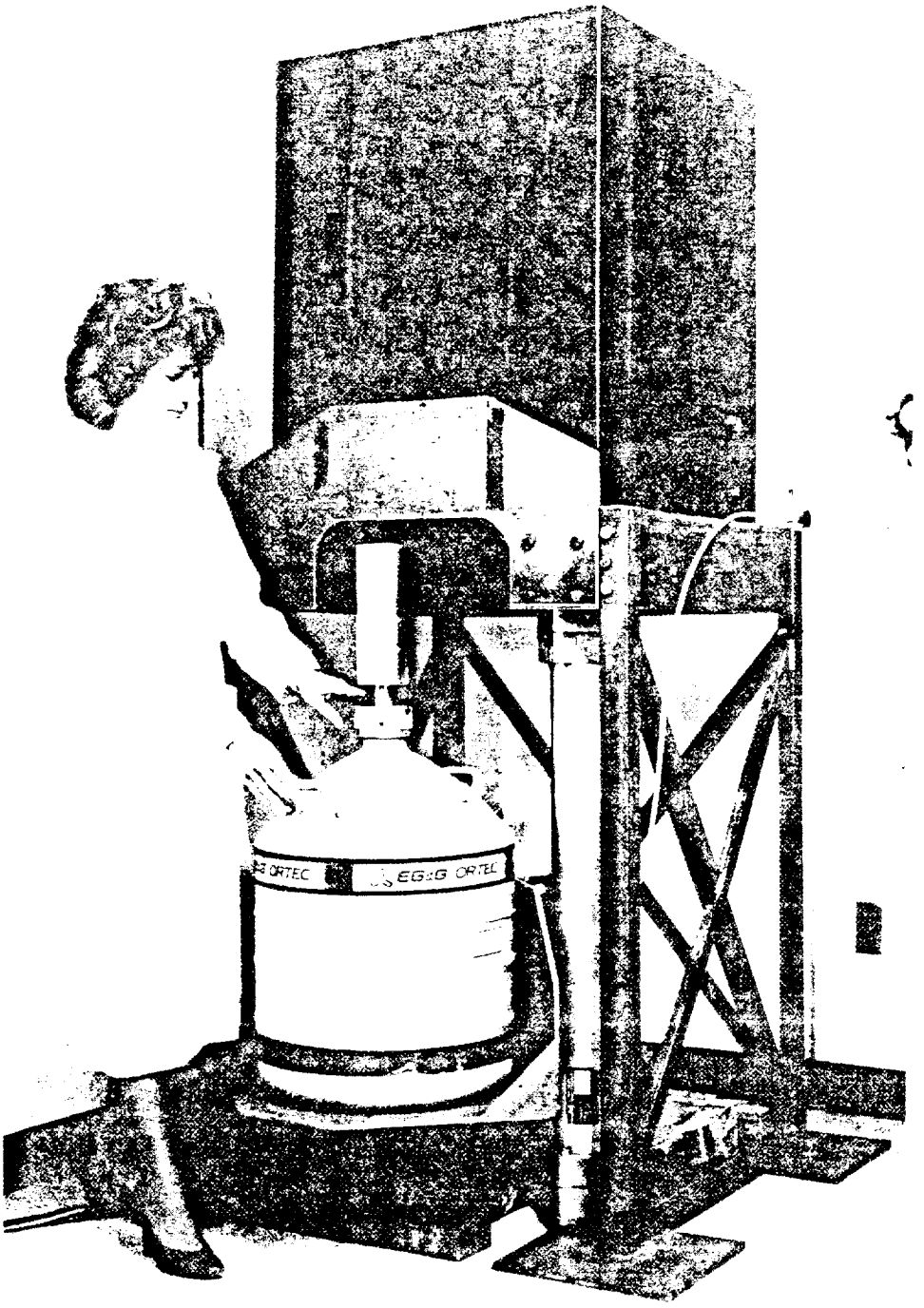

Fig. 2 Picture of Lead Shield

This system was designed for a quality control process for screening low background detectors, which required a design for easy exchange of various detector configurations. Even though the shielding design would not be considered state-of-the-art, there was a sufficient reduction of the ambient background to measure background levels of radionuclides. The reduction is similar to the more popular round shield produced by several commercial manufacturers.

The first step for measuring a detector after filling the 30 L liquid nitrogen dewar is to connect the bias supply, automatic shut-off and preamplifier cables. (See Figure 3 for block diagram). For optimum resolution the model 572 amplifier is set to a shaping time constant of 6 microseconds as specified on the detector data sheet. After the pole-zero is adjusted with a calibration source, as described in the amplifier operations manual, the system is ready for the calibration procedure.

The calibration procedure for the two-point calibration method is to count an NIST traceable mixed gamma radionuclide standard (SRM-4275b) of Eu-154, Eu-155, and Sb-125, for 3600 seconds at the same distance from the endcap (~10 cm.) The gain is set so that the 86.6 keV energy peak from Eu-155 is in channel 260 and the 1274.4 keV peak from Eu-154 is in channel 3823. Consequently, this provides for a gain of

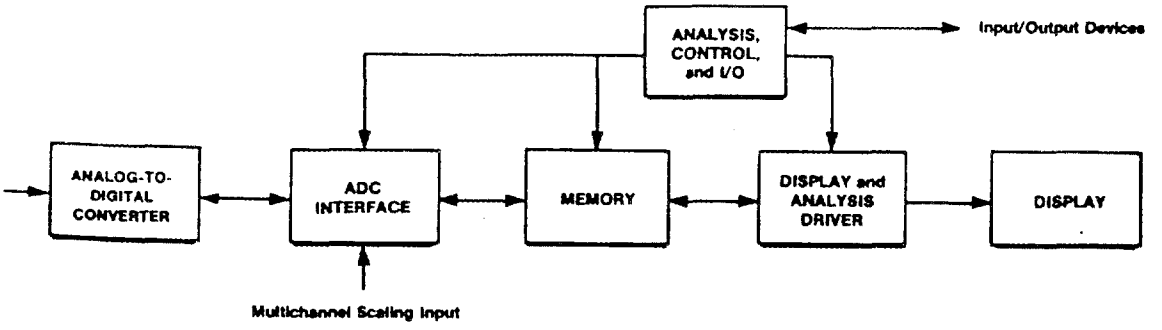

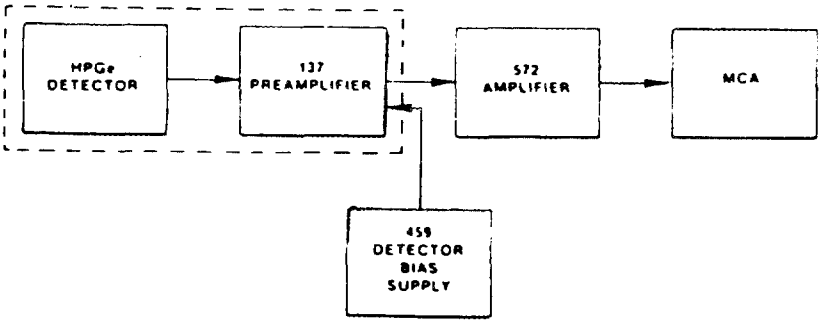

Fig.3 Simple Energy Spectroscopy System

0.33 keV/channel, yielding a full energy spectrum from approximately zero to 2700 keV. This energy range includes the Tl-208 peak commonly found in background spectra. (See Tables A.1 and A.2 in the Appendix for certification information for the source).[1]

After performing a two point linear calibration with the Maestro™ multichannel analyzer (MCA) emulation program, the channel file is transferred to the multichannel buffer (MCB) and saved to disk with the filename extension of P*cl.chn or P*c.chn (where * indicates a wildcard for the particular detector serial number) for future reference. The calibration source is removed and the display is cleared for acquiring the background spectrum. The preset for the livetime is set for 100,000 seconds. Then the detector is raised into the shield and the count started.

According to Cooper[1] it is very important to use equal counting intervals when comparing sensitivities of different spectrometers. For this reason only detectors which were counted for 3600 seconds for the calibration measurement were used for the FOM and MDA calculation and only background runs for 100,000 seconds were used for the LLD or MDA calculation. Attempts were made to normalize the calibration data for

---

[1]For future reference all tables may be found in the Appendix Section.

time, and were unsuccessful because the statistics are also affected by a different counting interval. However, a calibration run of at least 1000 seconds (greater than 10,000 counts in the calibration photopeaks) could still be useful for calibration purposes; thus preserving the usefulness of the background measurement. The list of detectors and their times can be seen in the raw data table in Appendix B.1.

After many detector background spectra were evaluated, a list was developed of the most commonly found nuclides. This list consists mainly of the uranium and thorium daughter products and Co-60 and Cs-137 (See Table A.1). A batch file software program called LBTABLE generated a region of interest (ROI) file with the associated energies and channels for the isotope list shown in Table A.1. The Low Background Analysis report generated the following information: region number, centroid energy (keV), start and stop channels, gross and net peak area, net % error, and the corrected counts/1000 sec. Information from this table provided part of the raw data necessary to calculate the LLD values for each of the background channel files.

4. SPECTRUM ANALYSIS

An EG&G ORTEC software program for gamma-ray spectrum analysis was used to generate the absolute efficiency values for the FOM and LLD equations. Basically, there are two steps required when using either the EG&G ORTEC OMNIGAM or MINIGAM software package for quantitative analysis, these are calibration followed by analysis.

The steps for calibration are as follows:

1. Calibration begins with a two-point energy calibration, followed by the creation of a library of nuclides and peaks used in the calibration and analysis. All peaks for Eu-154, 155 and Sb-125 were used for the calibration library and selected non-peak areas were chosen for both calibration and background spectra (See Table A.3 for standard source activity levels, Table A.4 for Calibration Library 4275b, and Table A.5 for Calibration Library for MDA 4275, and Background Library for MDA in Table A.6).
2. The analysis parameters are set in the GERPAR or germanium parameter analysis program. For MDA calculations the sensitivity for peak acceptance was set at 100%, with KTA Rule (see Equation 8 page 30) selected for detection limit method and background width determined from the best method of the 5-point, 3-point or minimum method. Also, the isotopic activity, isotope

and peak matrix, and energy and peak matrix report and decay correction to date for the calibration source are set here. No peak to background correction, random summing, or absorption corrections are used for these calculations, since the raw data is required without any corrections.

3. The channel file is converted to a spectrum file format, and merged with the calibration data file, sample description file, detector description file and analysis parameter files in the CONVERT program. This is shown in Figure 4 in the flow diagram for the analysis process.
4. The energy-efficiency calibrations are performed and transferred to the spectrum file using the CLB program.

The steps for analysis are as follows:

1. Save the background channel file and merge this file with the parameter file using the CONVERT program for each detector's calibration file. This step merges the analysis nuclide libraries file and the spectrum file also shown in Figure 4.
2. Start the analysis program AN1 and print the report.

4.1 Implementation of Software Analysis Program

As described in the OMNIGAM Software Manual[8], the software program analyzes the spectrum files and produces a

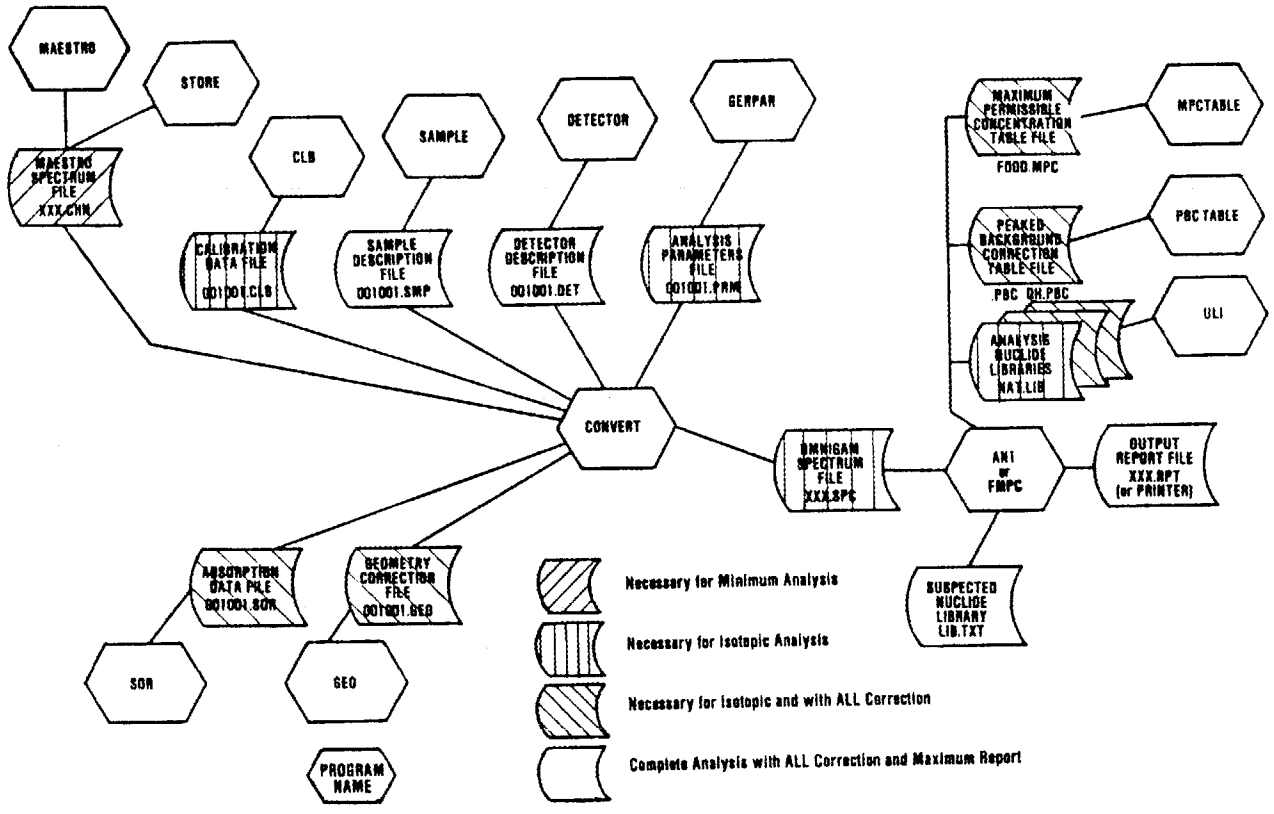

Fig. 4 Programs and Disk Files of B30

list of the background, net area, counting uncertainty, FWHM, and net count rate for all peaks in the spectrum. A list consists of:

1. the average abundances of the isotopes in the sample,
2. the abundance of each isotope based on each gamma-ray energy in the library,
3. the MDA for each peak energy of all the isotopes in the library,
4. and the reasons the unacceptable peaks were not used for the abundance calculation.

Also, on the same report peaks that are not the right shape are marked with a code indicating the reason the peak failed the peak shape test. Peak areas are also marked that are the result of deconvolution of overlapping energies and gamma-ray energies not in the analysis library and are reported as suspected nuclides if a match is found in the suspected nuclide library.

The report contains all the descriptions stored with the spectrum file including operator input descriptions, the analysis parameters, and the list of peaks and nuclides normally found in the spectrum.

4.2 Background Calculation

For the parameter file, the background calculation method was selected as the "best method" from a choice of

automatic, 5-point average, 3-point average or minimum method. Usually the automatic method is selected as the "best method".

The automatic method is based upon the peak centroid of the library energy value. The background calculation on the low energy side of the peak is from the peak centroid region to the 5-point average of the channels that are three times the FWHM below the peak centroid. The 5-point average is the sum of the data from two channels below this point, to two channels above this point, divided by 5. The background is selected as the minimum average point and is assigned to the center channel 5. The 5-point average is selected if the minimum average at this channel point is within one sigma of the actual channel value. If the average value is not within one sigma of the actual data, a 3-point average is used instead of the 5-point to calculate a new minimum value. If this 3-point value also fails the one sigma test, then the data value at that channel is used for the background. This entire process is then repeated for the high side of the energy peak. The background calculated is a straight line from the high to the low energy value.

By choosing the "best method" of analysis for background areas where there are no peaks, the 5-point average method will pass the one sigma test. The other methods will be

applied when there are other peaks in close proximity to the peak under consideration. Due to the lack of multiplets in the spectra being analyzed the best method would predominately be the 5-point with a few 3-point methods.

This is why careful attention was applied to the selection of non-peak areas of the spectrum when creating the non-peak libraries for both the calibration and background library files.

4.3 Creating Nuclide Libraries

Several nuclide libraries were created for analyzing the calibration and background spectra. Originally, there was only the calibration library (4275.LIB) based upon the nuclides listed in Table A.2 and the background library. However, two additional libraries were created for analyzing the MDA areas of the non-peak areas and these are listed in Table A.5 and A.6.

4.4 Calibration

The hard copy results are in the supplementary section. Both an energy calibration and an efficiency calibration were completed for each calibration spectrum in this study. This is in addition to the two-point calibration that was saved with the spectrum before beginning the background spectrum count.

The energy calibration calculates two sets of parameters: the energy versus channel numbers and the peak shape or FWHM versus energy. It is necessary to have a spectrum file and a library of peak energies. The library peaks are then fitted to the spectrum peaks and the peak channel centroids and library energies are fit with a linear least-square quadratic equation. For the calibration source about 12 peak energy values are used insuring a fit within 5% error and for most peaks this value was closer to a 1% error.

The result of this fit is a table consisting of: the input peak centroids, library energies, fitted energies, percent difference between the library and the fitted energy, peak FWHM, fitted FWHM and the percent differences between the peak and fitted FWHM. The energy versus channel and FWHM versus energy coefficients are stored in the calibration file records for further use by the efficiency calibration process.

The efficiency calibration calculates the detection efficiency as a function of energy. Factors affecting the detector efficiency are the detector itself, the detector-to-source geometry, the materials surrounding the detector and absorption in the source material or matrix. Since, all but the detector factor remained constant, the results of the efficiency calibration will yield specifically significant results in the subsequent analysis process.

As shown in Figure 5, p-type detectors have a maximum efficiency at about 150 keV. This is referred to as the knee value. The knee energy value is used in the efficiency calibration for fitting purposes of two different energies. The best fit value for the 4275B standard reference material was from 130 - 150 keV region where the efficiency starts to decrease after the maximum point. A quadratic fit was chosen for energy values above the knee and a linear fit was chosen for the few data points below the knee values. The resultant fit was checked with the calibration plotting feature for goodness of fit.

The absolute efficiency values from the energy-efficiency calibrations for each spectrum are then used in Equation 3 to acquire the LLD value at each photopeak energy of interest. Then the LLD value versus relative efficiency is plotted to show the inverse relationship.

The analysis process is also completed for regions of interest of known, non-photopeak areas of the background spectrum. These values are reported as the MDA values from the gamma spectroscopic software analysis program. The MDA value is similar in function to the LLD, however the MDA incorporates the resolution of the detector system unlike the LLD equation as the equations that follow show. The reported

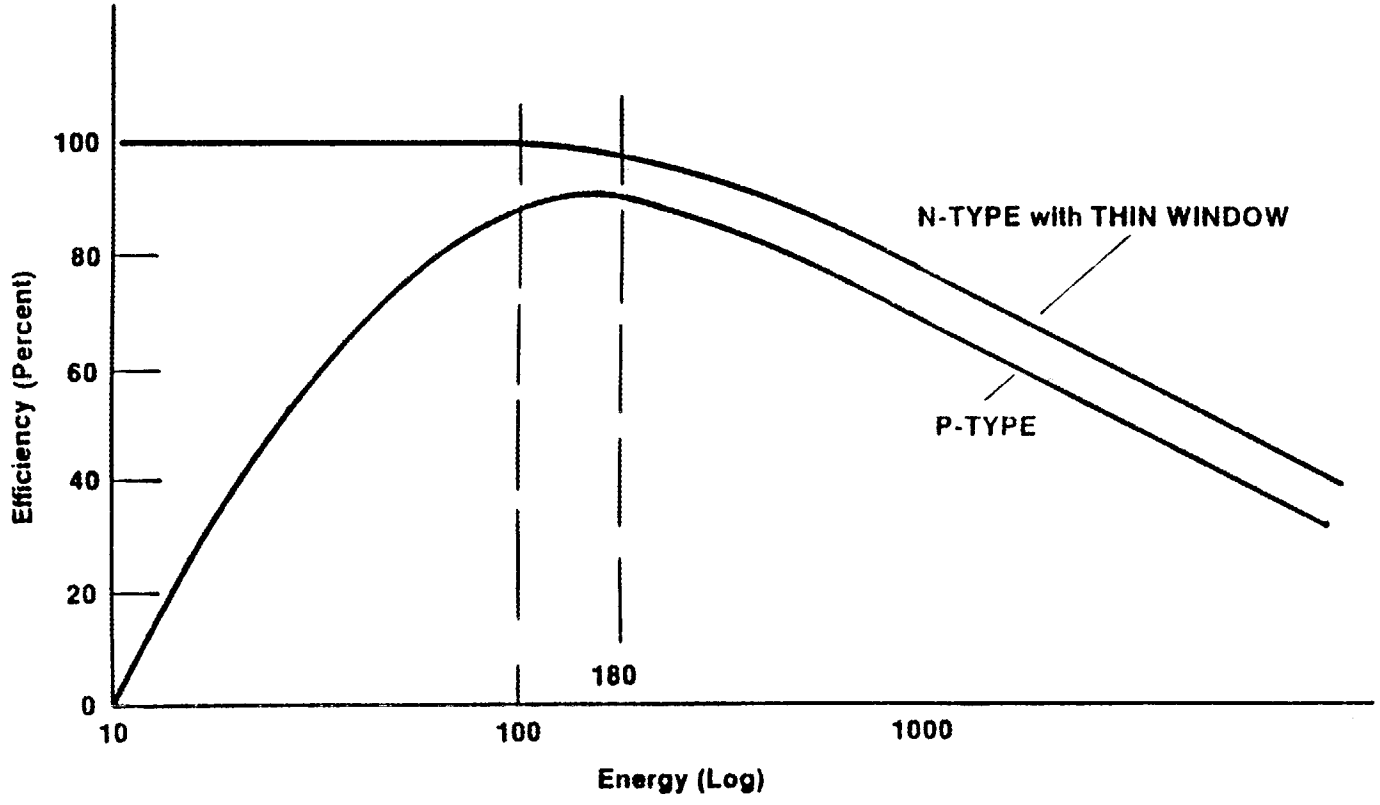

Fig. 5 Energy-Efficiency Curve

value for MDA using the KTA rule is based upon the following equation:

$$P = 2 \frac{\sigma * (B*W)^{\frac{1}{2}}}{t} \tag{8}$$

where,

P = peak count rate

W = number of counts in the (FWHM)

t = live-time of count

B = average background counts, counts/channel.

Then,

$$MDA = P / \Gamma * \epsilon = \frac{2 \sigma (B * W)^{\frac{1}{2}}}{t * \epsilon * \Gamma}, \tag{9}$$

where,

Γ = gammas per disintegration

ϵ = absolute photopeak efficiency.

This formula takes into account the resolution, allowing for analysis of the data directly, without needing to readjust for different resolutions. This is similar to the Figure of Merit calculation which also uses the FWHM value at a given energy. Therefore, using this formula to evaluate selected background peaks that had previously been evaluated with the LLD calculation shows a normalization of the data points.

For evaluation of the sensitivity comparison the derived MDA equation is used where

$$\mathrm{MDA} = \frac{[R(E_1)B(E_1)]^{\frac{1}{2}}}{\epsilon(E_1)} \quad . \tag{10}$$

This is similar to Equation (6) except here $B(E_1)$ equals $B_{c2}(E_1)$, since it is assumed the background is proportional to the Compton efficiency.[4]

5. RESULTS

The selection process as outlined in the Experimental Section was applied to approximately 200 detector measurements conducted from the period of September 1986 - October 1989. Selecting only p-type detectors narrowed the field down to about 125. Because the standard n-type detectors typically have a five fold higher background counting rate than p-type detectors they were deleted from this sampling. As mentioned earlier different geometries and shielding materials may also affect the detector efficiency or sensitivity. This narrowed the field down to only detectors measured in the same shield and the same geometry (streamline transplantable vertical (SV)). Also, there was a short period of time in 1987 when a slightly higher than normal background level of Co-60 was detected in the stainless steel material used for manufacturing the stainless steel flanges. Later in early '88 there occurred an increase in the Cs-137 background levels which was later found to be attributable to charcoal used as a pumping agent. The charcoal was contained in small aluminum cans and was originally used because it had a lower concentration of the uranium and thorium nuclides normally found in the more commonly used molecular sieve material. Since these detectors had a higher concentration of a high energy radionuclide, the associated Compton continuum would also be

increased, resulting in a conflicting sensitivity comparison. This deleted a few more measurements from the possible total to about 30 for the final study.

Table B.1 shows the values for the parameters that are used as performance indicators for the detectors in this study. This table also shows that increasing the relative efficiency generally increases the peak-to-Compton,[9] however this is only a direct correlation when the resolution (FWHM) also improves. These differences are translated into the FOM and LLD versus efficiency graphs indicating wide differences for comparable efficiency data points. This can be seen most noticeably when several similar efficiency data points are plotted for either FOM or LLD as shown in Figures 6 and 7. As previously mentioned the graph of LLD versus Efficiency shows an increasing improvement for the LLD until a plateau is reached around 70-80 % efficiency.

The FOM values from Figure 6 appear to fluctuate less than the LLD in Figure 7 for similar efficiency detectors. The FOM is based upon the 3600 second calibration measurements and the LLD is based upon the 100,000 second background measurement. The improved statistics for the higher count rate partially explains the wider fluctuations for the LLD versus efficiency graph. But, most importantly, is the fact that the resolution is included in the FOM

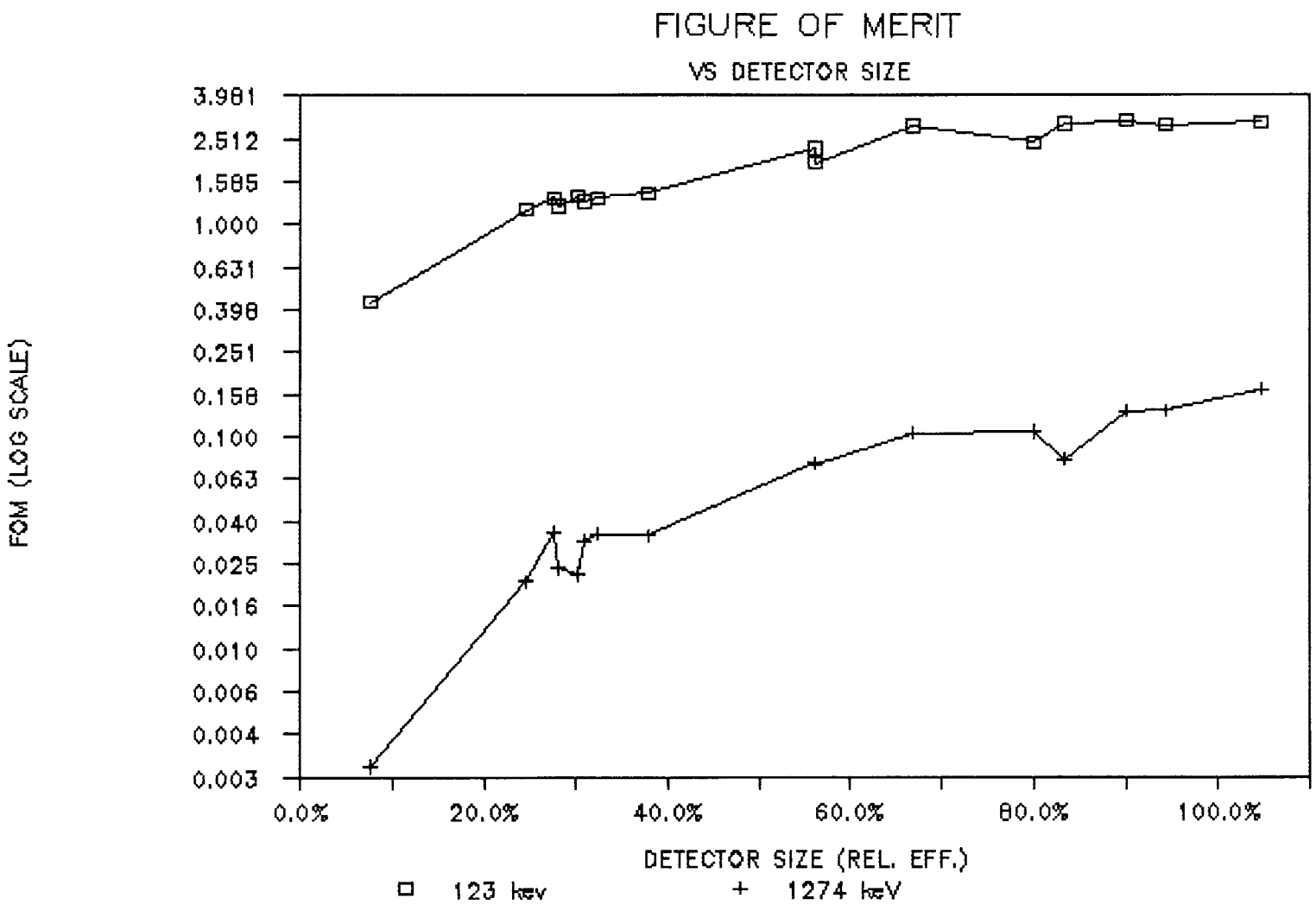

Fig. 6 Figure of Merit (FOM) versus Detector Efficiency

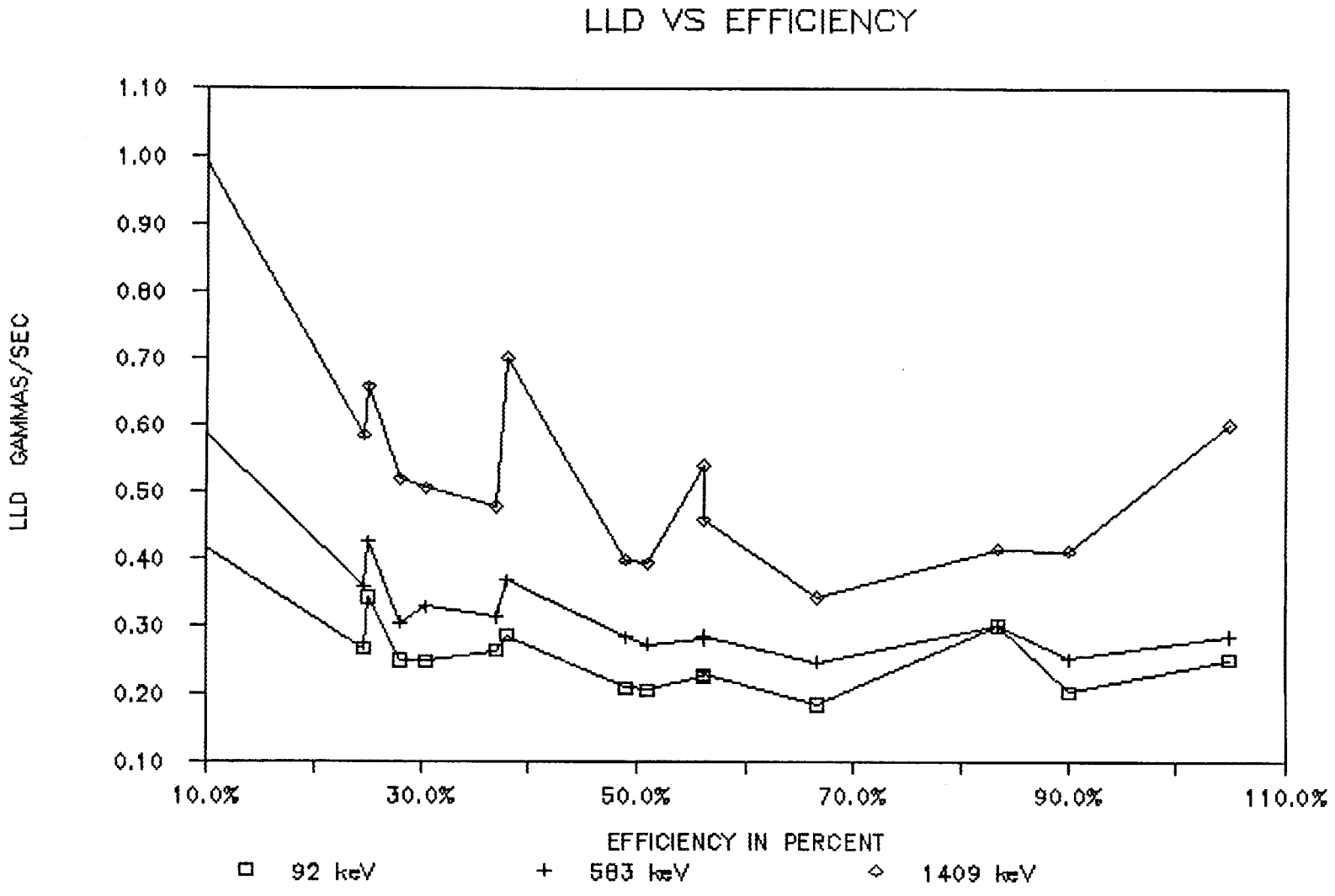

Fig. 7 LLD versus Efficiency

equation and not in the LLD equation. The FOM allows for a normalization of the detectors performance.

As shown in Figure 8, where peak-to-Compton is graphed as a function of energy, there exists a generally increasing function up to about 80% for the standard configuration detectors. The poor peak-to-Compton of 74.8 for the 105% relative efficiency detector probably results from the poor resolution value of 2.36 FWHM for the Co-60 peak. A similar peak-to-Compton is shown for the 49% relative efficiency detector which has a value of 75.9 for the peak-to-Compton and a resolution of 1.72 keV FWHM. The energy resolution is determined by a combination of three factors: the inherent statistical spread in the number of charge carriers, variations in the charge collection efficiency and contributions from electronic noise. According to Knoll,[2] the energy of the radiation and the size of the detector determines which of the factors dominates. At low energies the contribution from electronic noise and charge collection dominate, and at higher energies the additional broadening is due to charge carrier statistics. Small volume detectors usually show a better energy resolution due to two factors. First, lower capacitance values, and the electronic noise of the system increases with detector capacitance. Secondly, the effects of carrier loss due to trapping are magnified in

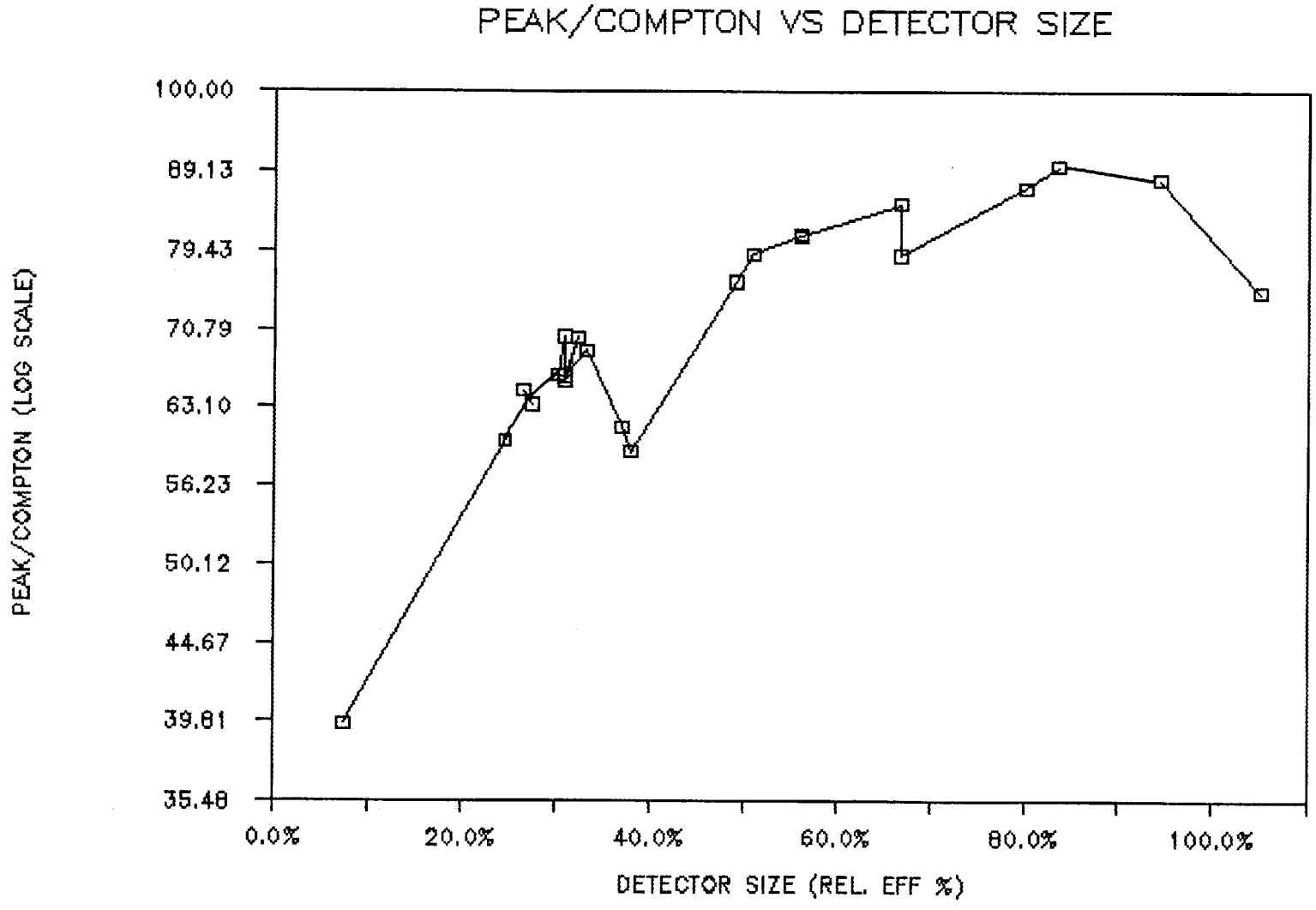

Fig. 8 Peak-to-Compton versus Energy

large-volume detectors with relatively large collection distances.

Energy resolution is one factor that explains the graph as shown in Figure 7 where a 50% detector acquires comparable sensitivity measurements to a 90% detector. Another contributing factor is the increased efficiency of the larger volume detector to see the background radiation from the detector cryostat materials of construction.

5.1 Detection Efficiency

By definition, a detector's efficiency is equal to the number of output pulses for each quantum of radiation that interacts within the detector's active volume.[2] In this study counting efficiencies are subdivided into two classes: absolute and intrinsic. Absolute efficiencies are defined as:

$$\epsilon_{abs} = \frac{\text{number of pulses recorded}}{\text{number of radiation quanta emitted by source}} \qquad (11)$$

The absolute efficiency is dependent upon both the detector properties and the counting geometry. The absolute efficiency value is used in the calculation for the FOM for the calibration measurements and the LLD for the background measurements. According to Knoll,[2] the intrinsic efficiency is defined as

$$\epsilon_{int} = \frac{\text{number of pulses recorded}}{\text{number of quanta incident on detector}} \qquad (12)$$

which does not include an implicit factor for the solid angle subtended by the detector.

The two efficiencies for isotropic sources are related by

$$\epsilon_{int} = \epsilon_{abs}(4\pi / \Omega) \tag{13}$$

where Ω is the solid angle of the detector as seen from the actual source position.[2] The intrinsic efficiency depends on the detector material, the radiation energy, and the physical thickness of the detector in line with the incident radiation. All these factors should be relatively the same, since the detector material is the same for all detectors (p-type), the same low background lead shield was used for all tests and all detectors were situated 10 centimeters from the endcap. However, with different efficiency detectors a slight dependence exists between the source distance and the frontal detector area, because the average path length of the radiation through the detector changes with this spacing. This becomes more apparent with the larger efficiency detectors because the ratio of the frontal area to length of the detector decreases as the following solid angle equations demonstrate.

For a point source located along the axis of a right circular cylindrical detector, the solid angle is given by[2]

$$\Omega = 2\pi \left(1 - \frac{d}{(d^2 + a^2)^{1/2}}\right) \tag{14}$$

where, d = source detector distance

a = detector radius.

For $d >> a$, the solid angle reduces to the ratio of the detector plane frontal area (A), visible at the source, to the square of the distance

$$\Omega = \frac{A}{d^2} = \frac{\pi a^2}{d^2} . \tag{15}$$

These measurements are all based upon a point source geometry for the calibration spectra. This geometry configuration may bias the FOM and MDA values in favor of the smaller efficiency detectors at the lower energies. This is because the smaller efficiency detectors tend to have crystals with a larger diameter-to-length ratio. A custom made Marinelli beaker standard source configuration test should minimize this bias. However, for the purposes of measuring background sensitivity the point source calibration configuration is appropriate as defined above for intrinsic efficiency.

The graph in Figure 9 of the FOM versus efficiency for the low background detector data shows almost no change at the higher energy values. However, the 123 keV energy shows a much larger difference ranging from 2 to 1.3 for detector sizes ranging from 44% to 40% relative efficiency. Figure 10

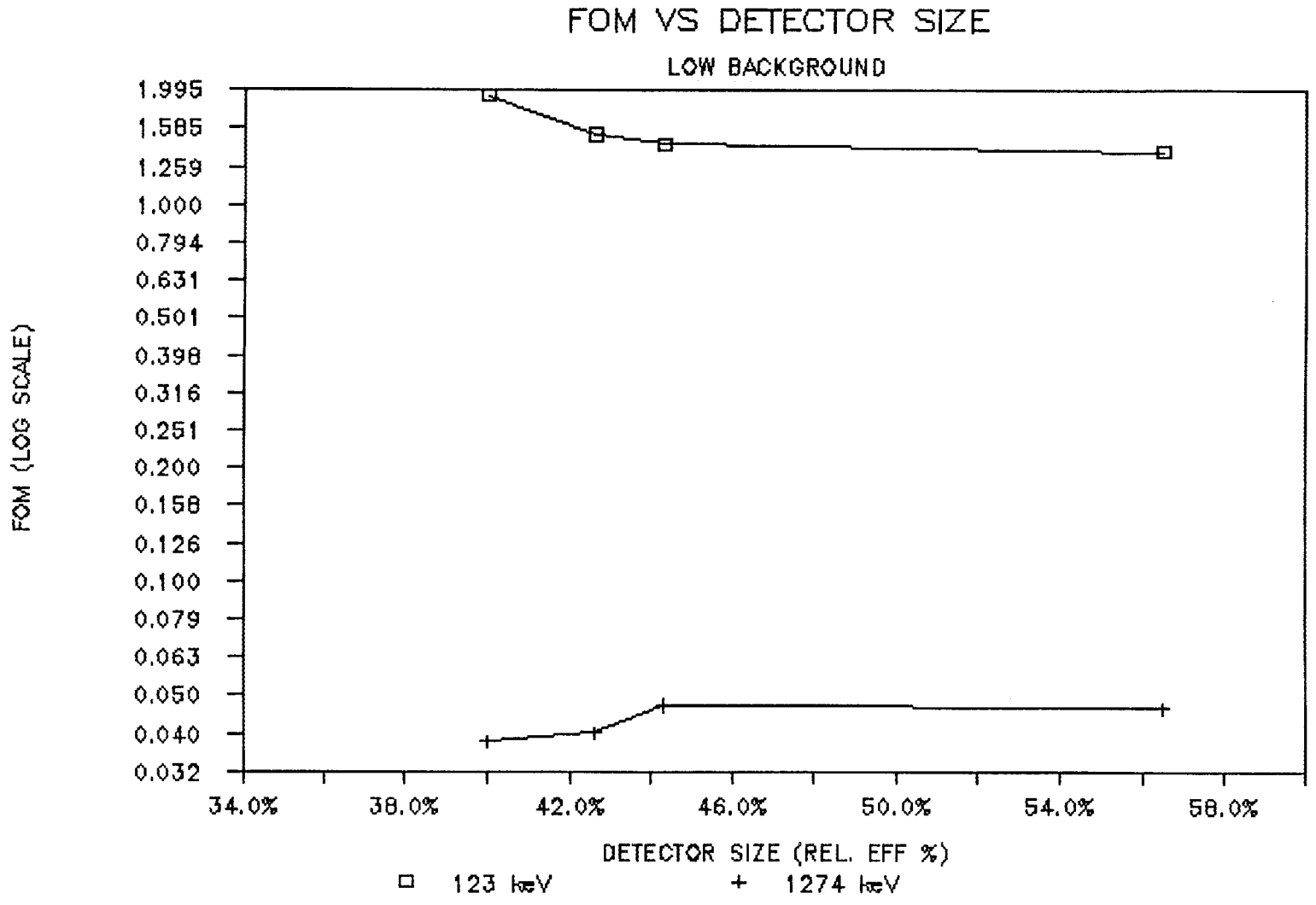

Fig. 9 FOM versus Efficiency

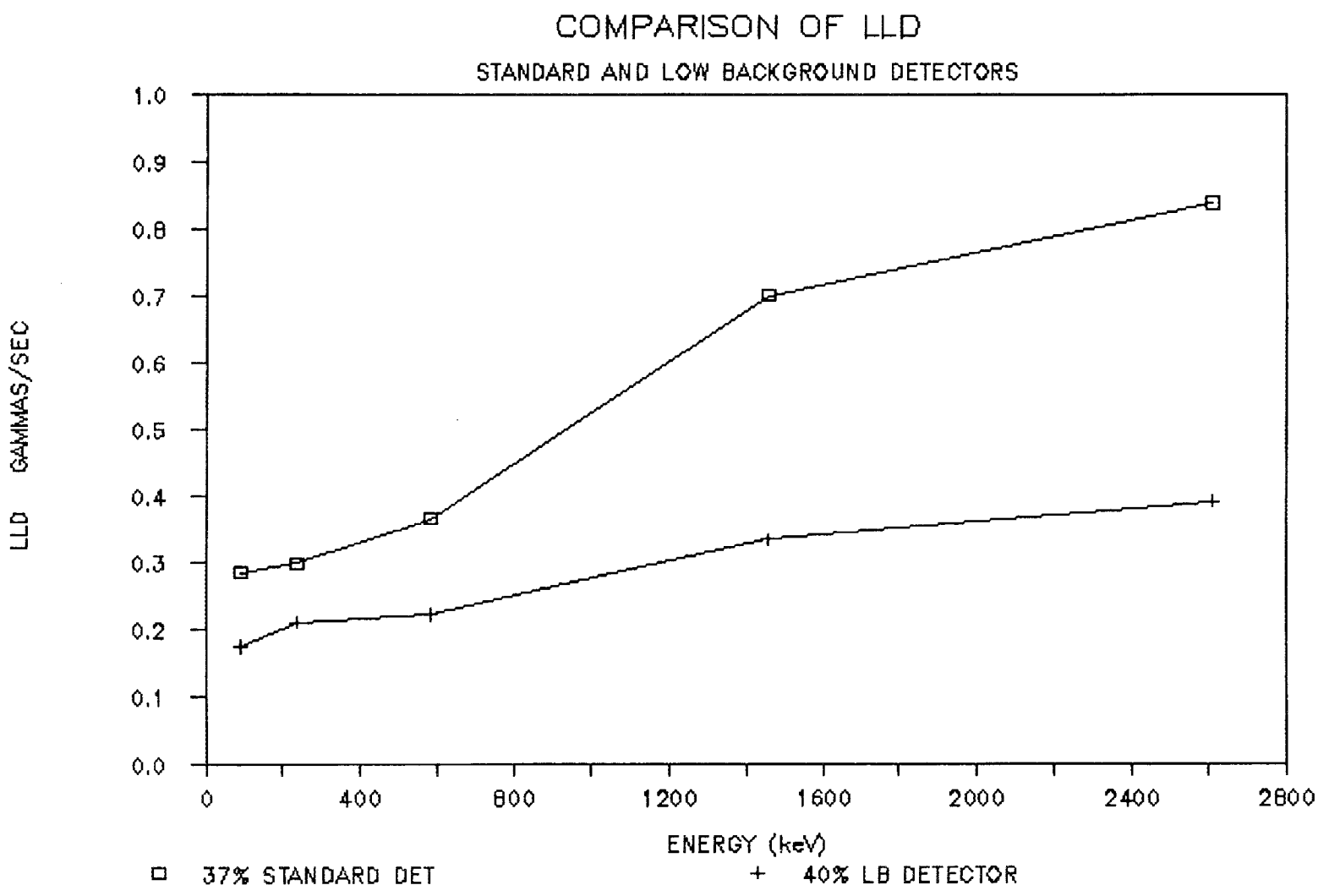

Fig. 10 Comparison of LLD for Standard and LB Detectors

compares a low background and standard detector for similar efficiencies in the graph of LLD versus energy. More than a 50% improvement in LLD is acquired with the low background detector at the higher energies.

The comparison of two similar efficiency and resolution detector is shown in Figure 11 for LLD versus energy for similar efficiency detectors. The differences are minimal between the two almost identical detectors, confirming that the variances are smaller for low background rather than standard detectors and that the experimental process is consistent. Figure 12 shows a graph of the standard and low background 56% detectors demonstrating the significant difference between the two types of detectors.

The calibration data used to generate the derived MDA values versus Energy graph are illustrated in Figure 13. This shows an increasing trend beginning at 500 keV and reaching a maximum at 750 keV. Several fundamental relationships must be used to explain this unusual graph. The first factor is based on the function of efficiency versus energy as shown in Figure 5. The increased efficiency at the lower energies supports the initial lower MDA value. The energy-efficiency curve reaches a maximum around 150 keV and then decreases linearly from that value. This rapidly decreasing efficiency causes a concurrent rise in the MDA

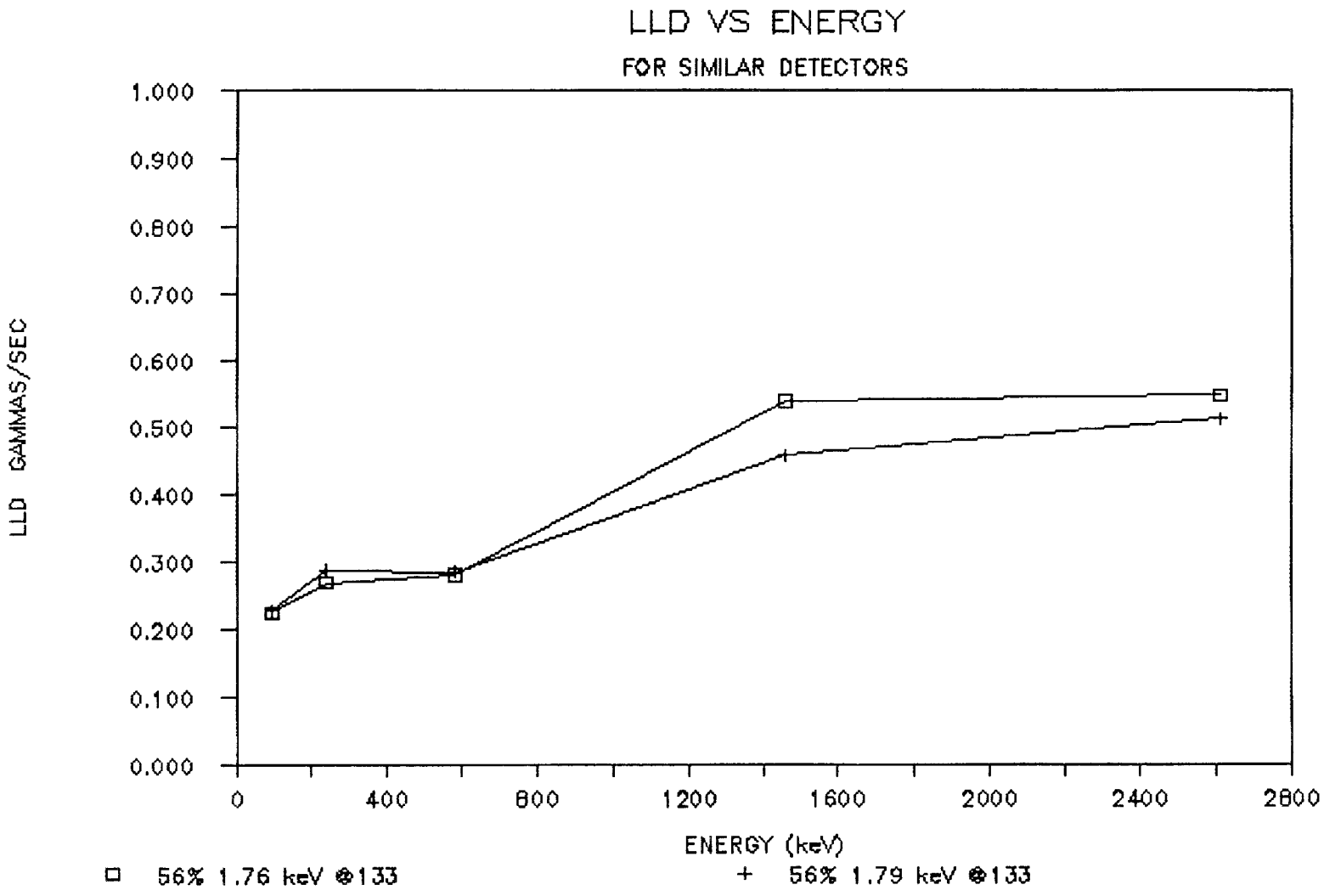

Fig. 11 LLD versus Energy for Similar Resolution

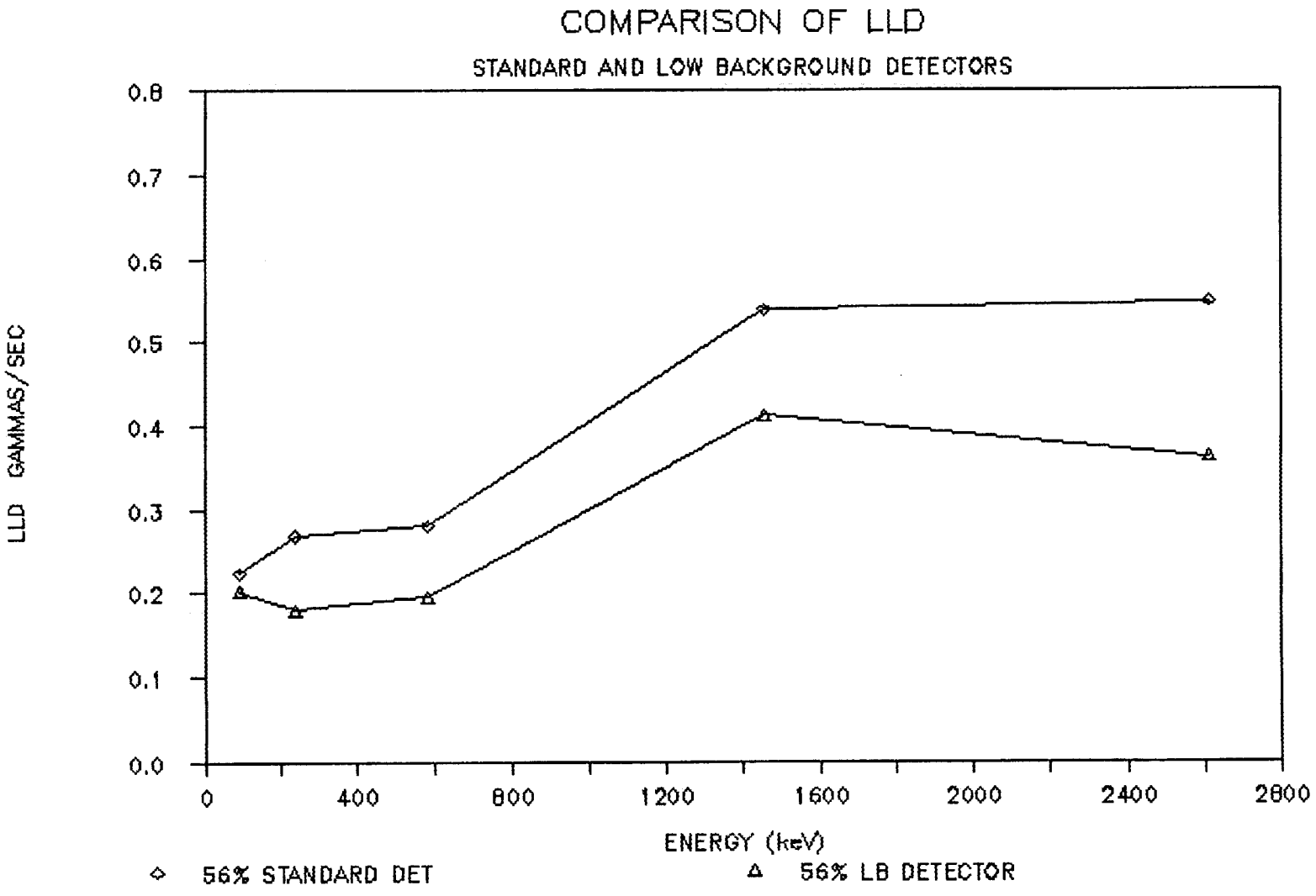

Fig. 12 Comparison of LLD for Standard (56%) and LB Detectors

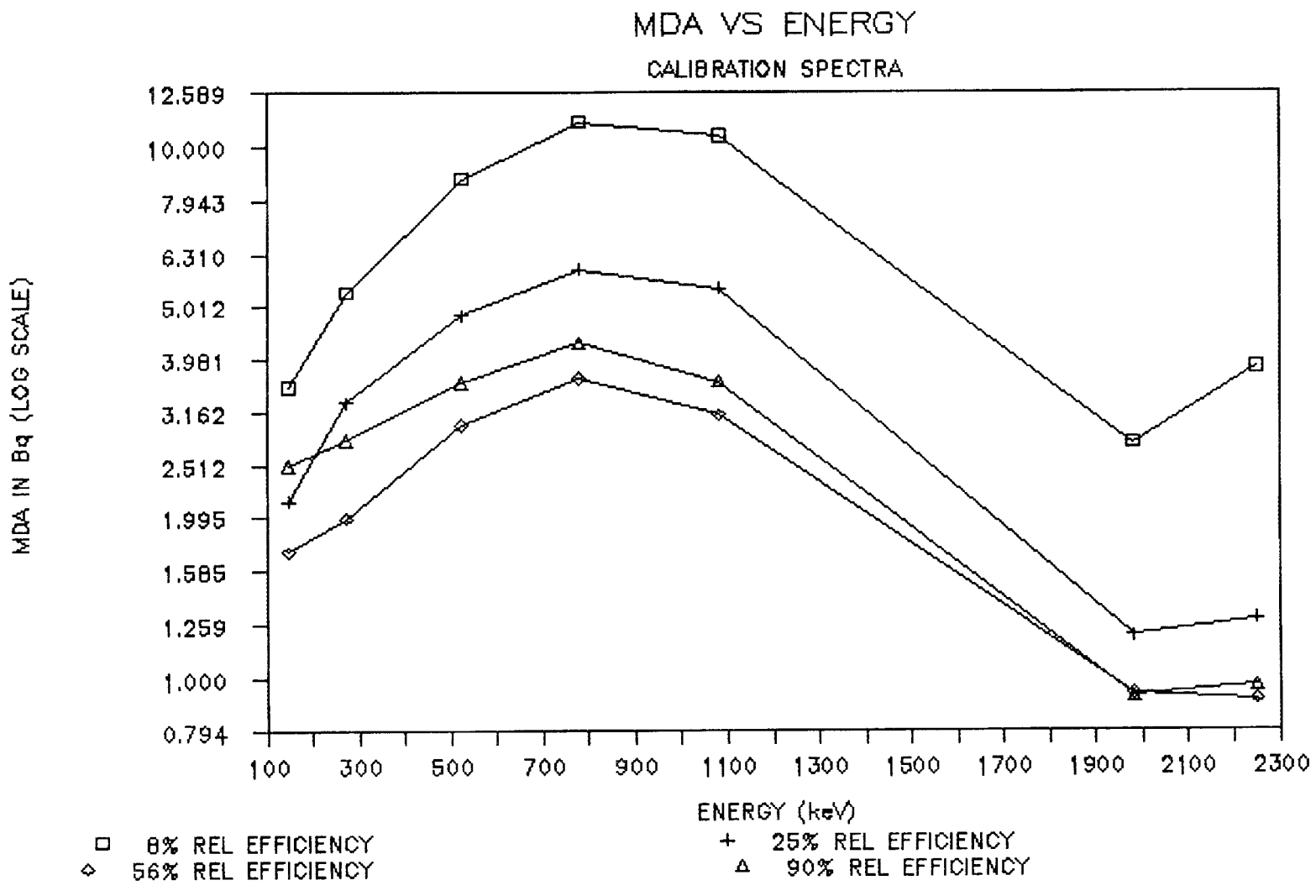

Fig. 13 MDA versus Energy for Calibration Spectra

versus energy graph. Additionally, the Compton background rate of change remains stable in this energy region, which allows the diminishing efficiency value to dominate the resultant MDA value.

Figure 14 shows how the MDA values vary for 220 keV, 700 keV and 2300 keV energies for background spectra. The most dramatic change occurs for the 25% efficiency and again for the 66% efficiency detector data.

The background values for peak regions of interest are also graphed in Figure 15. This graph shows slightly higher MDA values for the peak areas as one would expect. However, the 80% detector appears to perform the best at the 1238 keV peak; giving much better performance than any of the energies in Figure 14.

Non-peak ROI plots of the calibration spectra for MDA versus efficiency (Figure 16) indicates several inflection points. These are at ~30% efficiency, for 150 keV, ~43% for 525 keV, and ~67% for 2250 keV. If resolution and background remain essentially constant then the greater the efficiency, the better the improvement in MDA at higher energies.

Another way of examining the effects of energy on efficiency is shown in Figure 17 for MDA versus Energy.

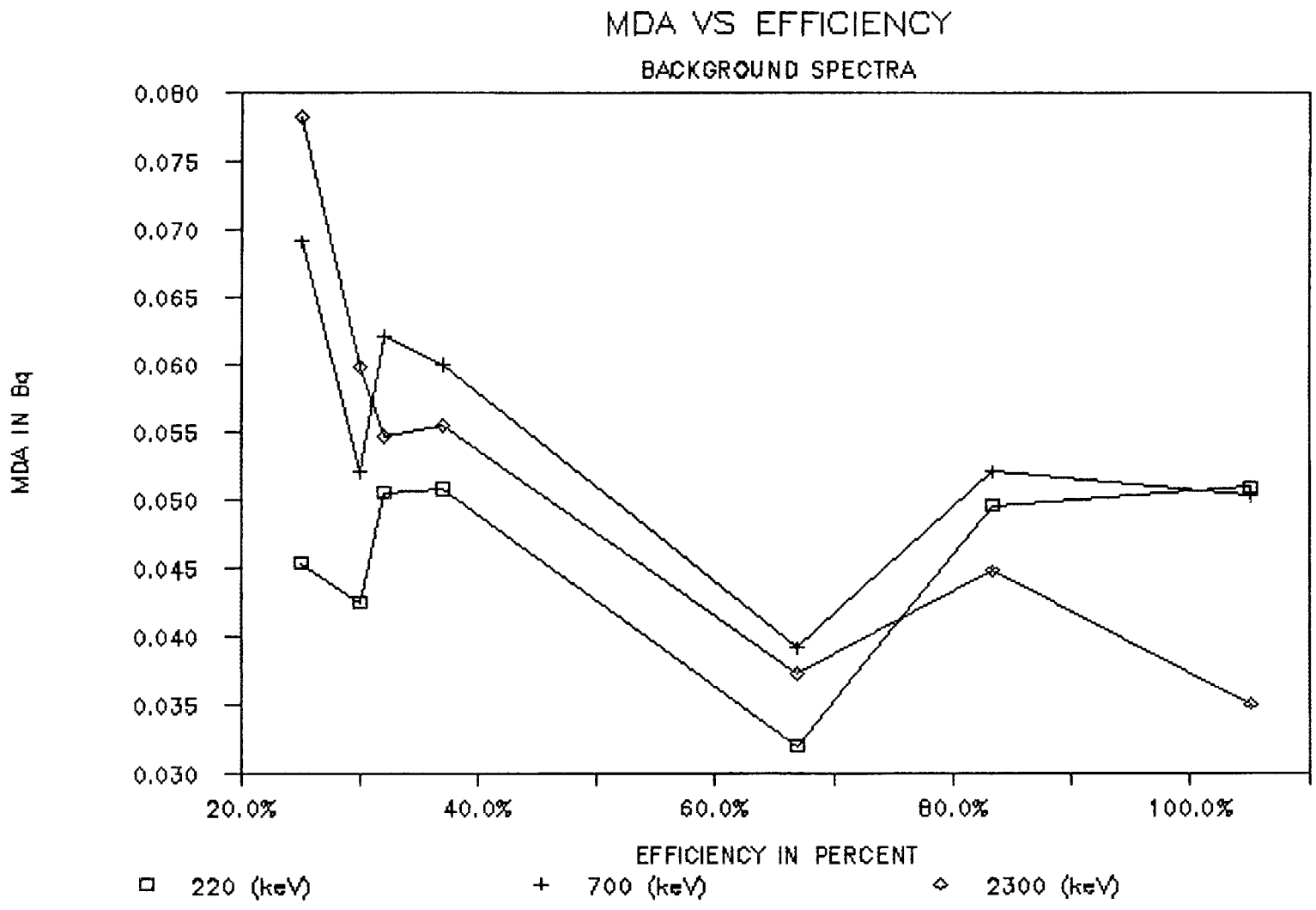

Fig. 14 MDA versus Efficiency for Background Spectra

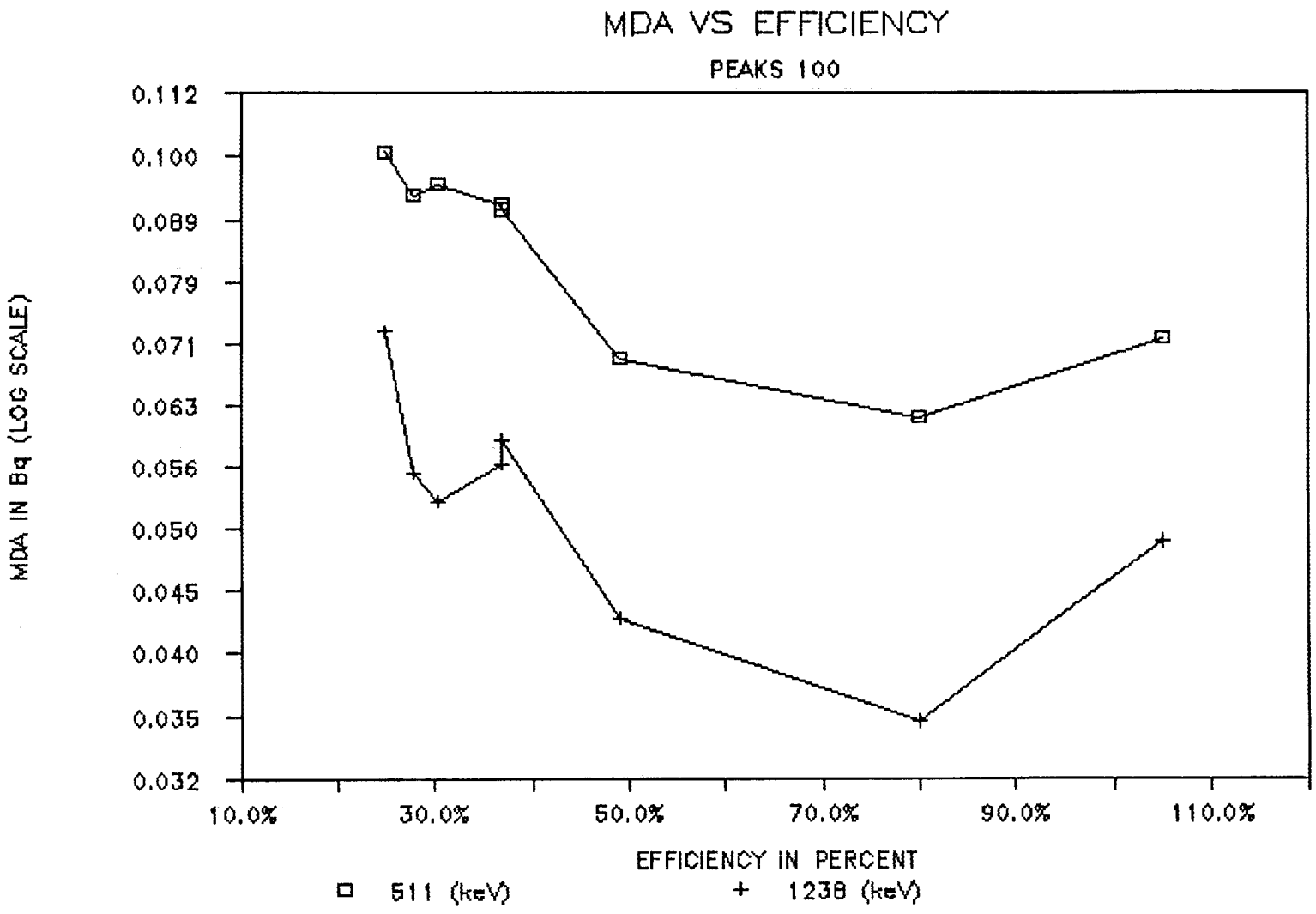

Fig. 15 MDA versus Efficiency for Background Peaks

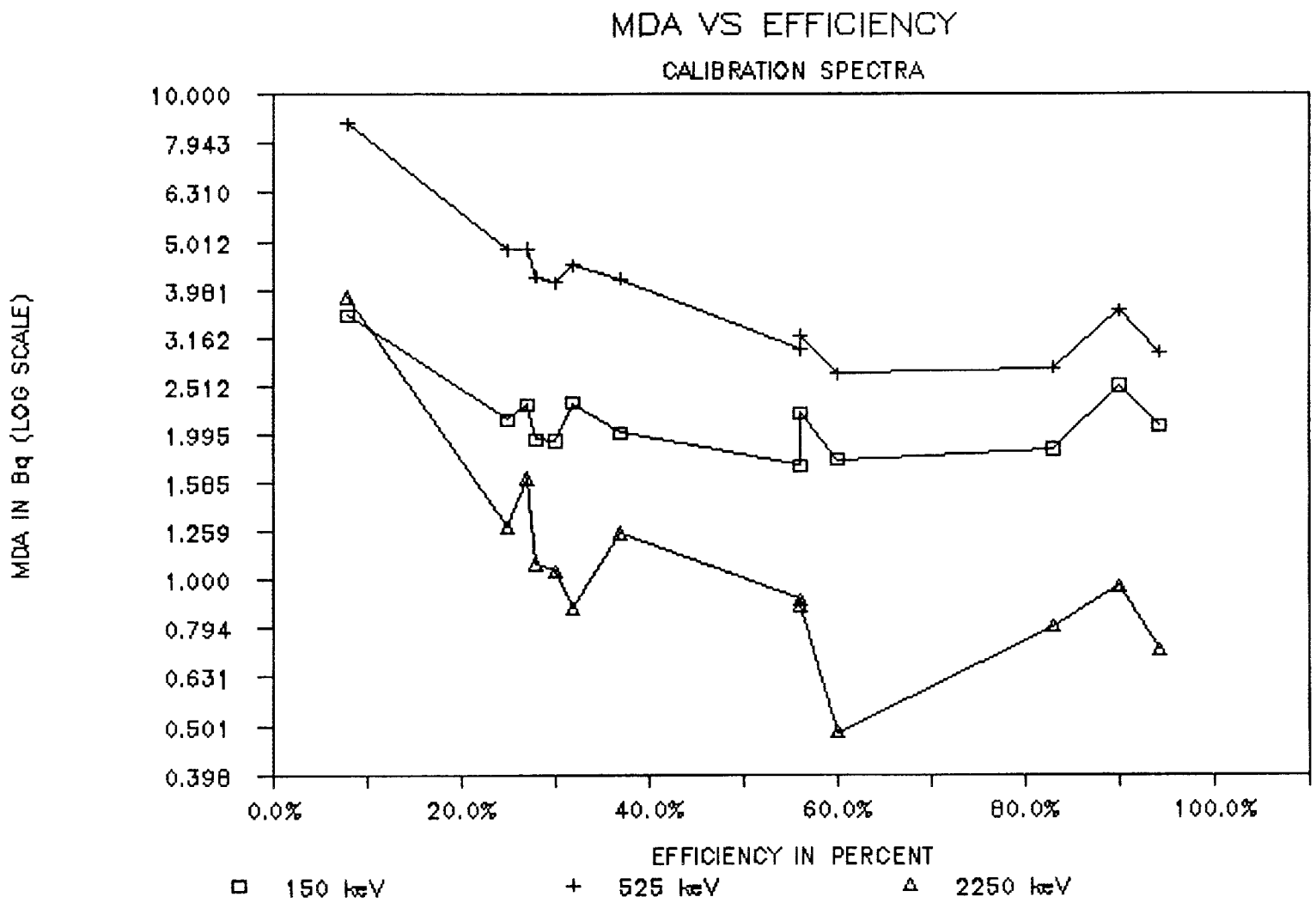

Fig. 16 MDA versus Efficiency for Calibration Spectra

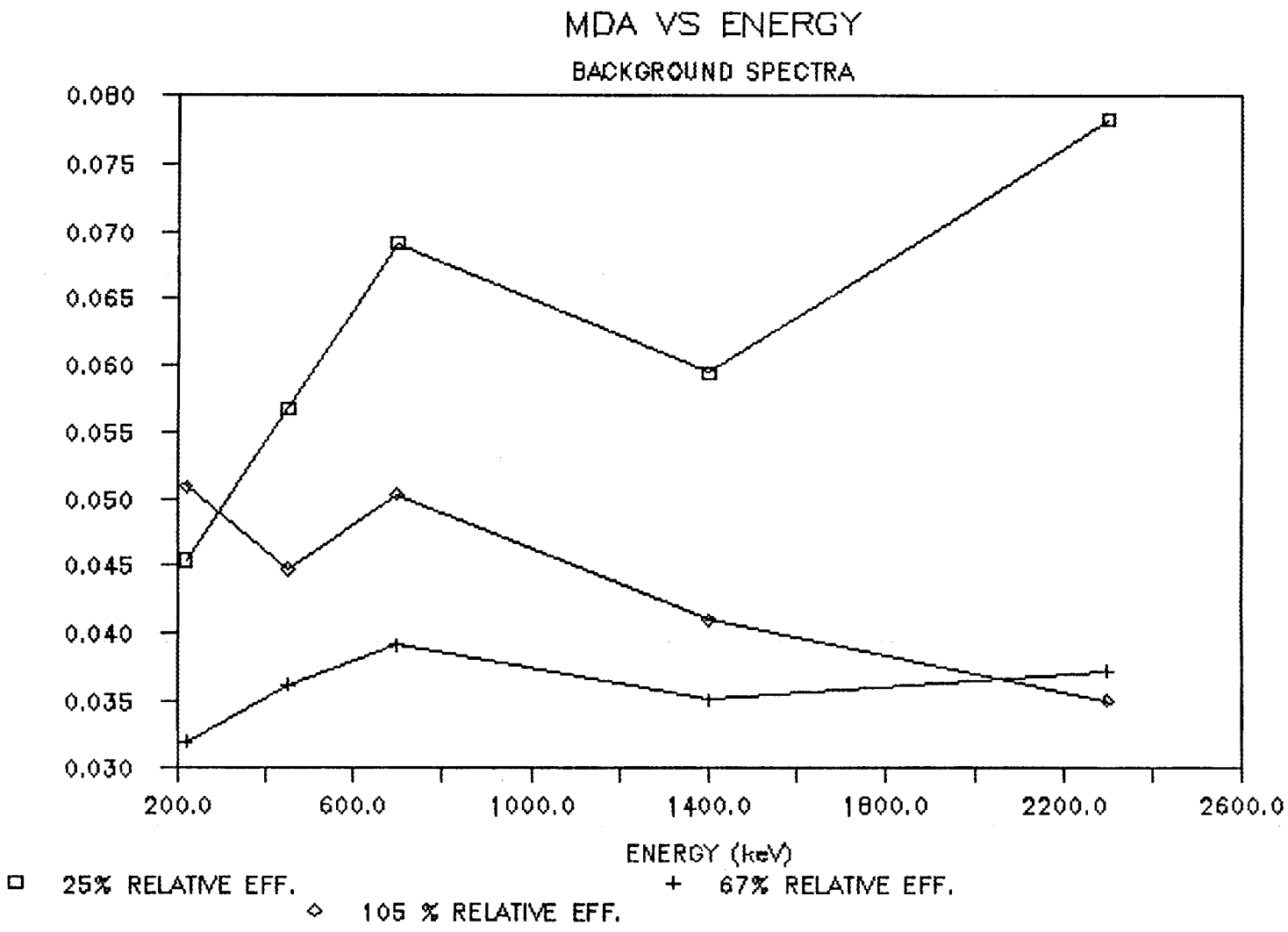

Fig. 17 MDA versus Energy for Background Spectra

This background spectra exposes the lower MDA for the 67% detector rather than the 105% detector. The poor performance of the 105% detector is due to a combination of factors, such as poor P/C, poor resolution and a crystal shape with a small diameter to length ratio.

An interesting comparison of MDA and LLD is shown in Figure 18. Originally, the MDA value was not divided by 4.66 and appeared similar to the LLD values except higher by a constant value. The overlay of the LLD value at 238 keV as a straight line over the MDA/4.66 (+) point values confirms that 4.66 is the constant value. There were not MDA values for all the LLD values, but the detectors graphed were similar in efficiency. Once again a plateau was reached around 70% efficiency. Increasing the efficiency beyond 70% achieves only marginal improvements for sensitivity. A series of background count time tests were conducted with an 83% detector (serial number P20149) at 10,000, 20,000, 60,000, 80,000 and the standard 100,000 seconds. The LLD values are plotted for the 93 keV and 1461 keV background peaks in Figure 19. The LLD values for this detector realize a 50% reduction from 10,000 to 20,000 seconds and almost no further improvements from 80,000 to 100,000 seconds. The count time versus MDA graph in Figure 20 is for the non-peak areas of the spectrum. A crossover between the 700 keV and the 220 keV energy occurs between 10,000 and 20,000 seconds,

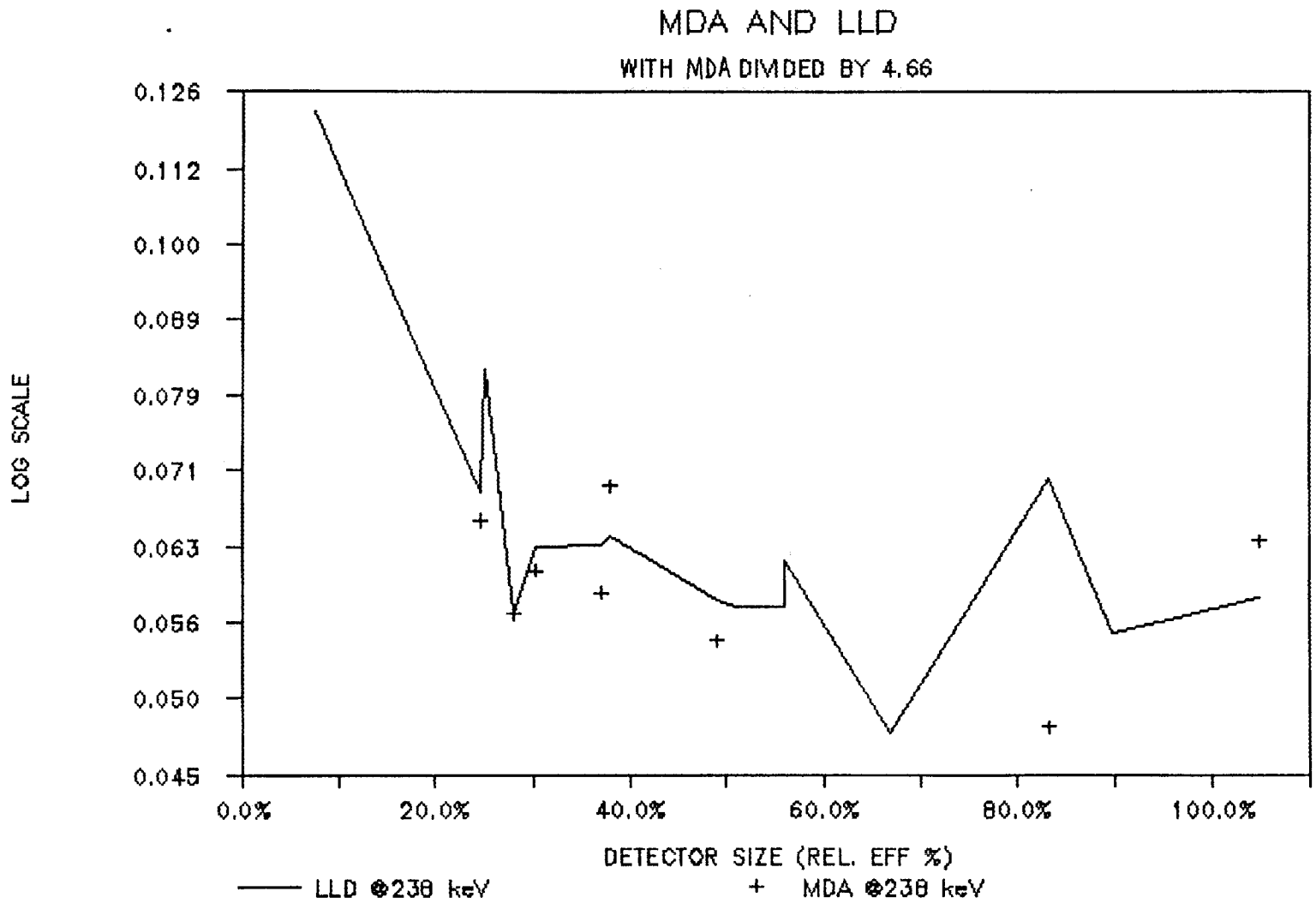

Fig. 18 MDA and LLD Comparison

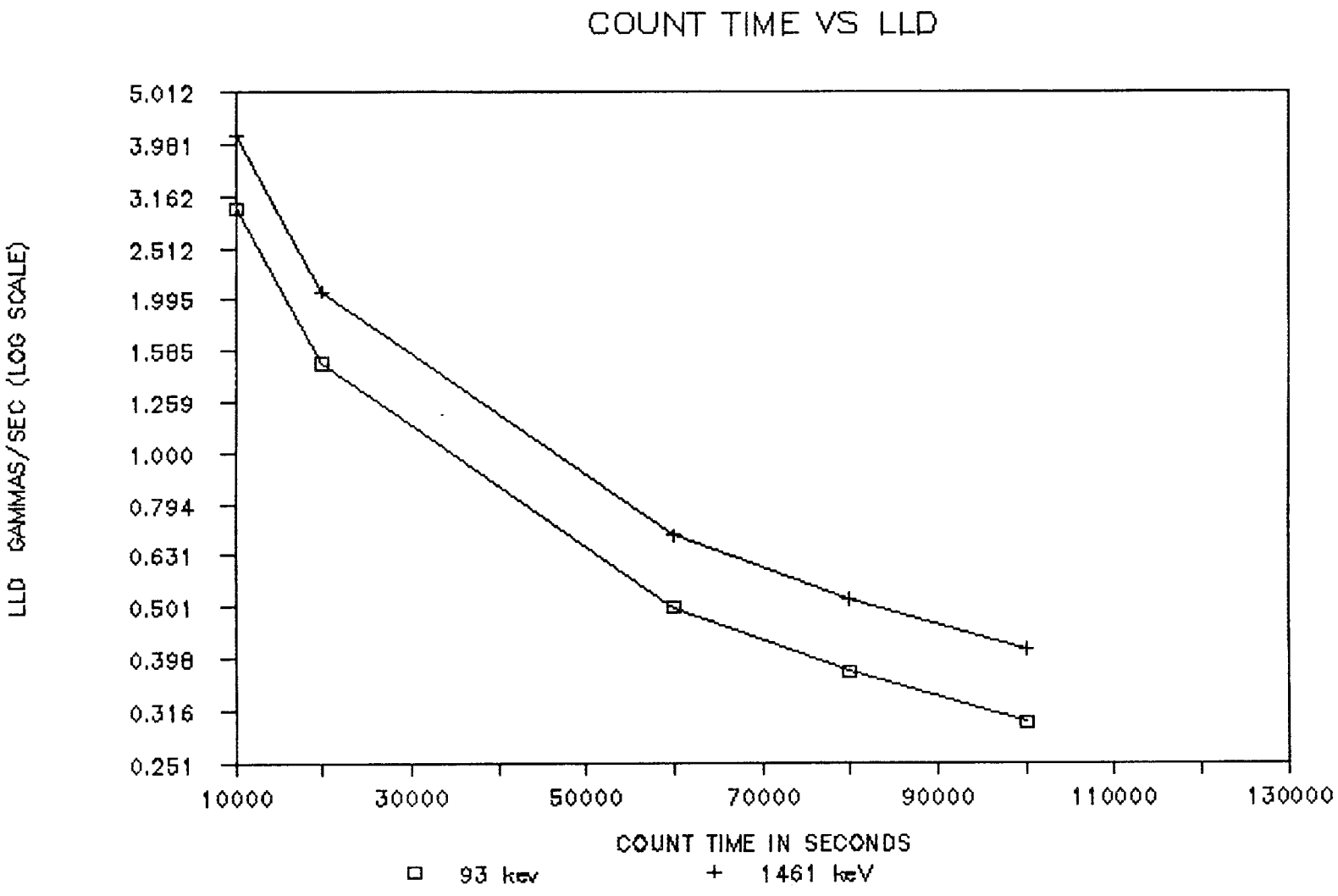

Fig. 19 Count Time versus LLD

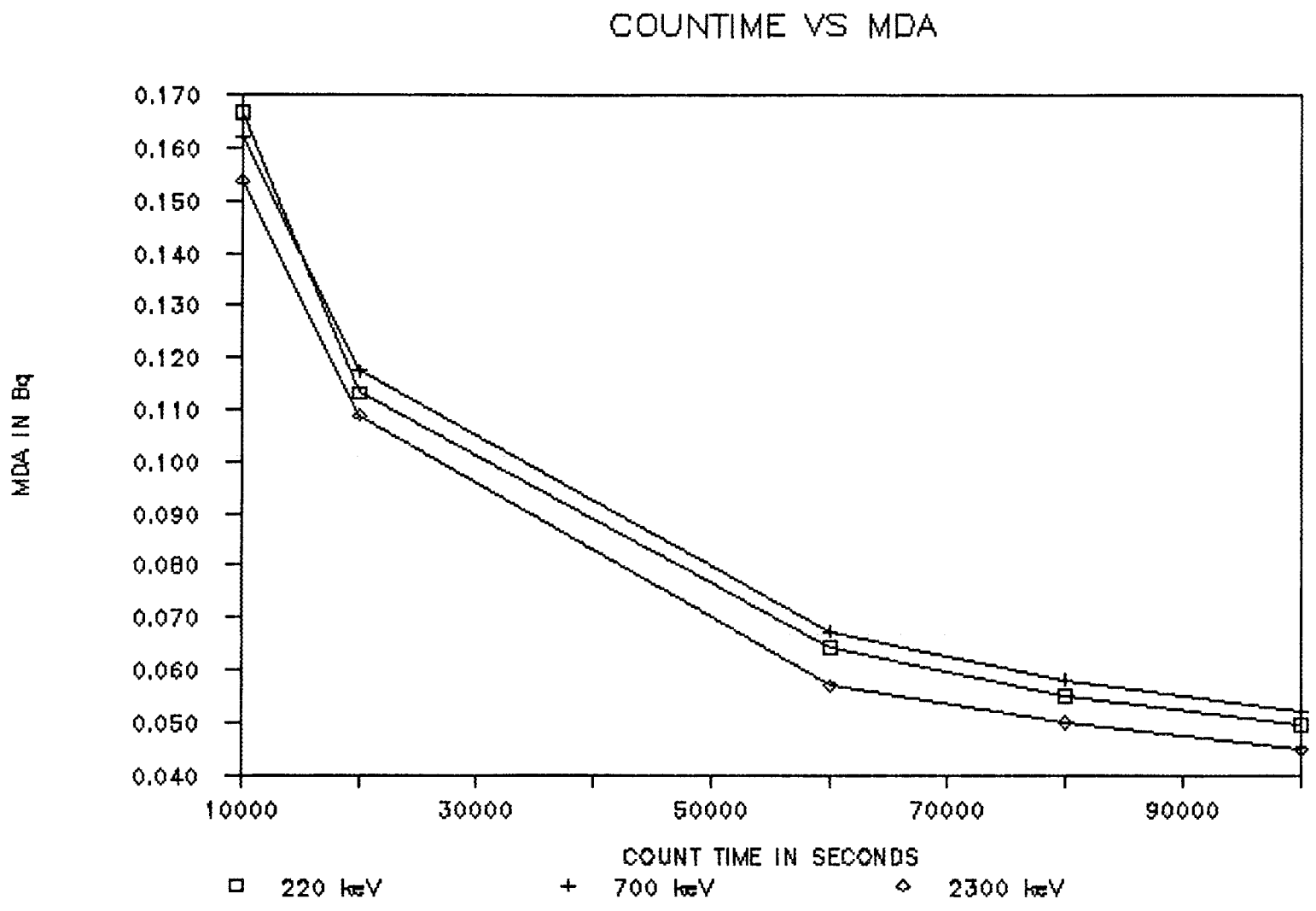

Fig. 20 Count Time versus MDA for Different Energies

showing that an additional 10,000 seconds improved the lower energy count at a faster rate. The same data from the MDA analysis of different count times is provided for the FOM by inverting the MDA values. This is illustrated in Figure 21 to give an approximate idea of the expected trends.

A representative sampling of three detectors was chosen from the detectors which were analyzed for MDA. Then applying the ratio between the measured 100,000 second and the other count times a relative list of values was generated for two additional detectors. A 23%, 37%, and the measured 83% detector were graphed for the energy values of 220 keV, 700 keV, and 2300 keV in Figures 22, 23, and 24 respectively. The lowest energy showed the lowest MDA value for the 23% detector which demonstrates the value of a 25% detector for the lower energy range. However, at 700 keV (as shown in Figure 23) the 83% detector indicates a 17% reduction in count time over the 37% detector and close to a 34% reduction in count time when compared to the 23% detector. The 83% detector also excels at the highest energy range exhibiting a 50% reduction in count time for the 20,000 second count as shown in Figure 24.

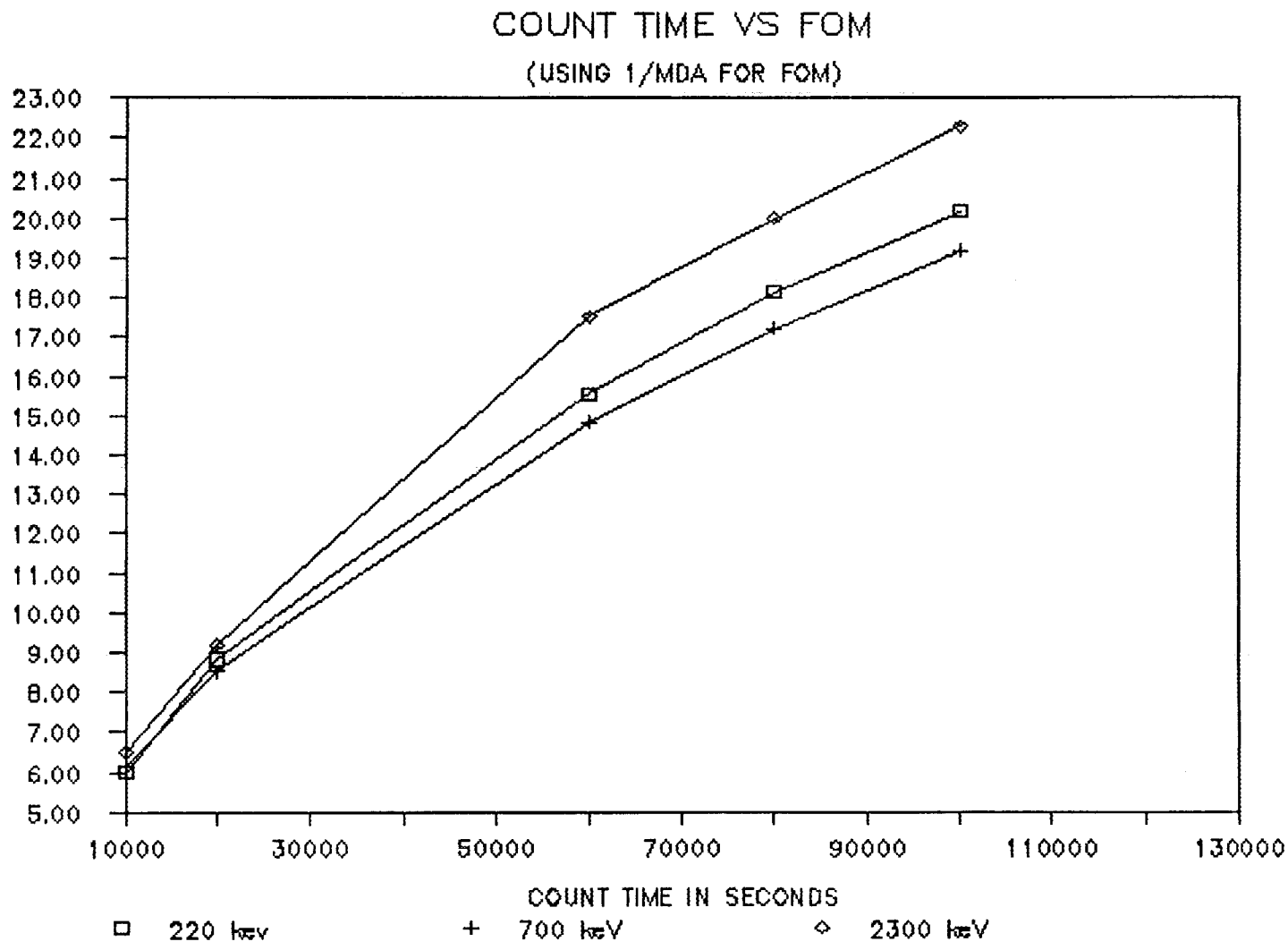

Fig. 21 Count Time versus FOM

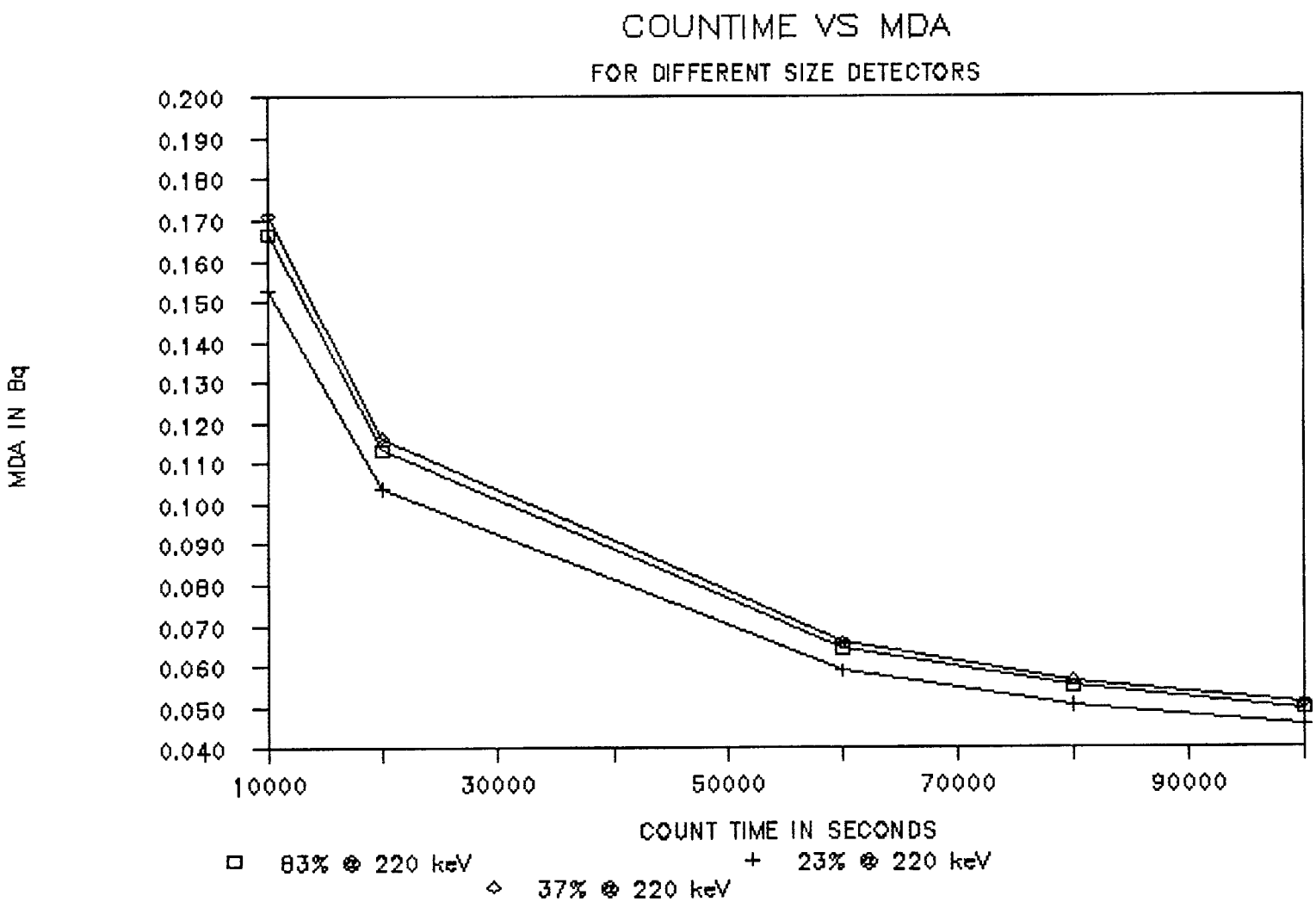

Fig. 22 Count Time versus MDA for Different Eff. at 220 keV

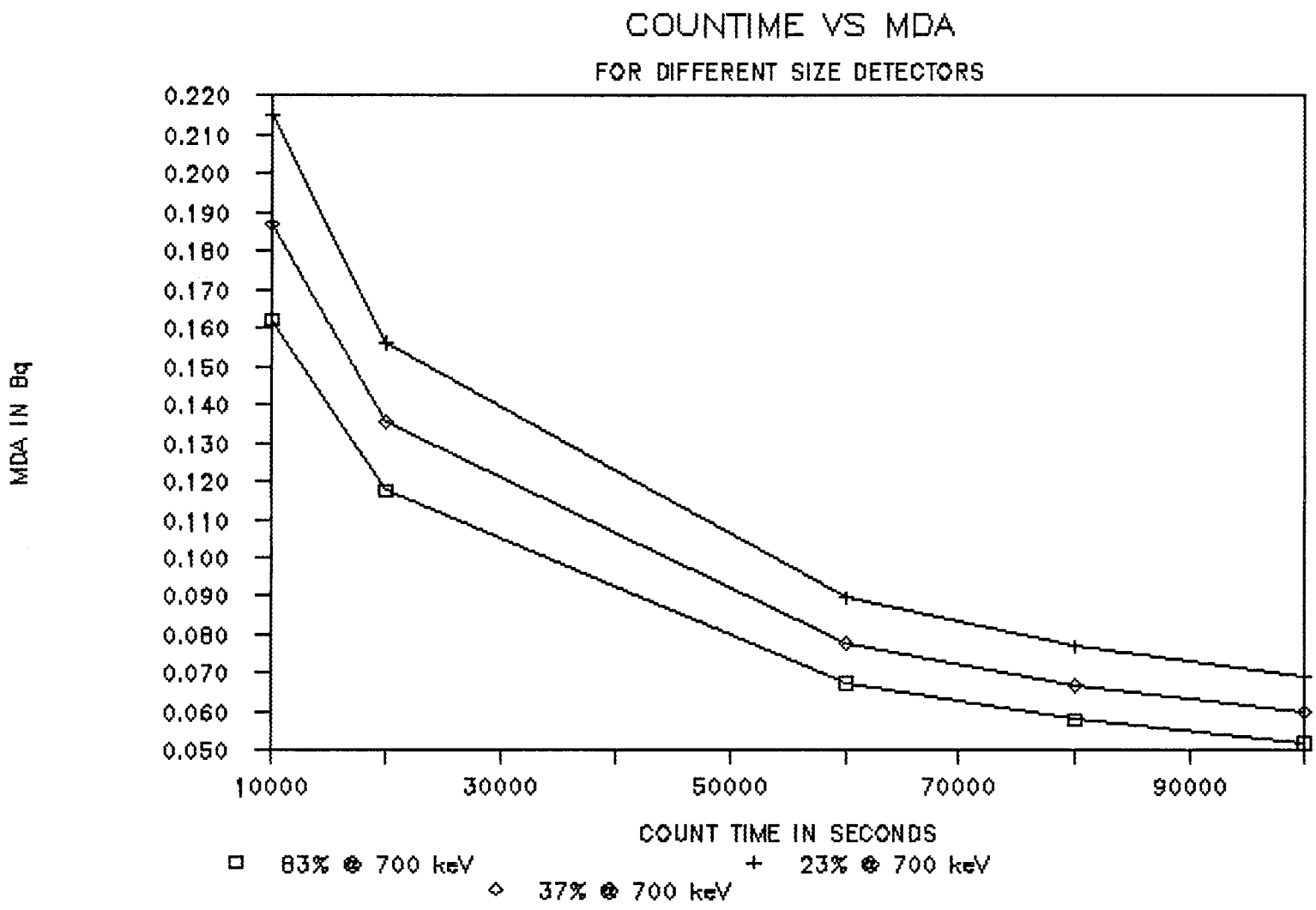

Fig. 23 Count Time versus MDA for Different Eff. at 700 keV

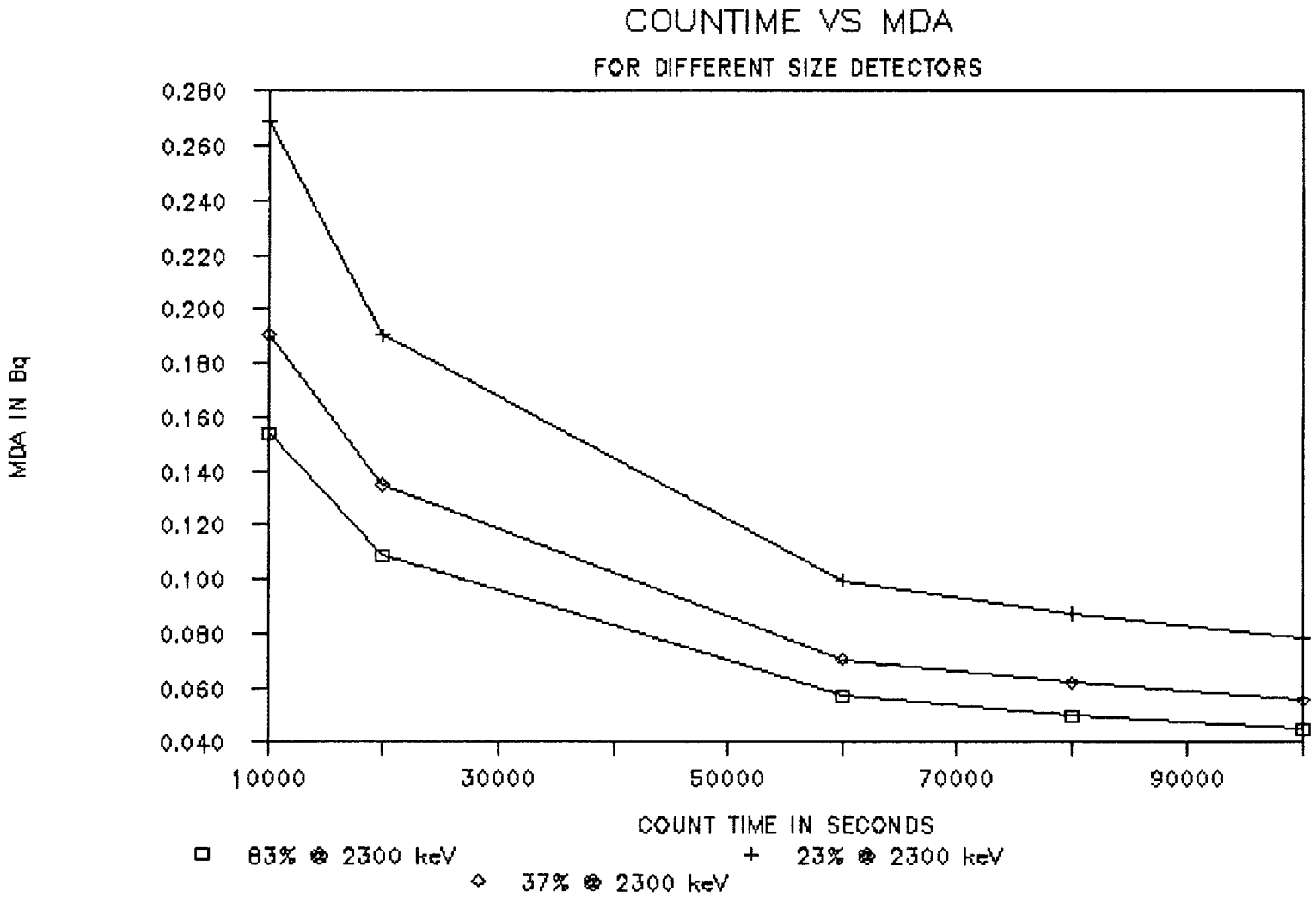

Fig. 24 Count Time versus MDA for Different Eff. at 2300 keV

6. CONCLUSIONS

This study indicates that in addition to the efficiency, the resolution, background, peak-to-Compton (P/C), and crystal shape of a p-type detector are of paramount importance when considering the parameters of a detectors' performance. The resolution value is included in both the FOM and MDA equation and indirectly in the LLD calculations (through the inclusion of absolute efficiency). The increase in background is most evident at the lower energies as shown by the graphs of efficiency versus energy. The P/C parameter is a measurement that combines both resolution and background, and in this study, improvement appears to plateau around 80%. Generally, the crystal shape of a smaller efficiency detector has a larger diameter-to-length ratio making its sensitivity greater for the lower energy nuclides. The larger efficiency detector diameter is limited by production practices, resulting in smaller diameter-to-length crystals, which have an advantage only at the higher energies.

The FOM values are most useful for a comparison of sensitivity measurements using calibration spectra, rather than background spectra. This is because the FOM calculation requires peak areas with a high count rate to ensure that the statistical error is small. The FOM in Equation 7 is only

valid when the statistical error (A_m) value in Equation 5 is small in relationship to the Compton efficiency for that peak. The results of the FOM versus energy at 123 keV indicate diminishing returns for efficiencies greater than about 50%. The higher energy calibration data at 1274.4 keV indicate a maximum value for the FOM around 80% relative efficiency. Since there is only a minimal improvement for efficiencies greater than 80% at the high energy range, the best choice of detector would not necessarily be the largest unless the higher energy nuclides are of particular interest (Figure 25).

The data generated by the MDA analysis of various efficiency detectors showed an unexpected rise for the MDA values around 750 keV. At this energy the maximum difference occurred for different efficiency detectors which would also result in a maximum difference for the count time. Therefore, the energy range requiring the highest sensitivity determines the performance indicators specified. For instance, if analyzing for low-levels of Cs-137 at the 661.6 keV energy, the higher the efficiency the better as shown by the MDA versus Energy graph . Providing that the resolution is relatively constant when compared with a "good" resolution 25% detector. Also, if efficiencies greater than 50% are being considered a low background detector will further increase sample through-put. Conversely, as stated earlier,

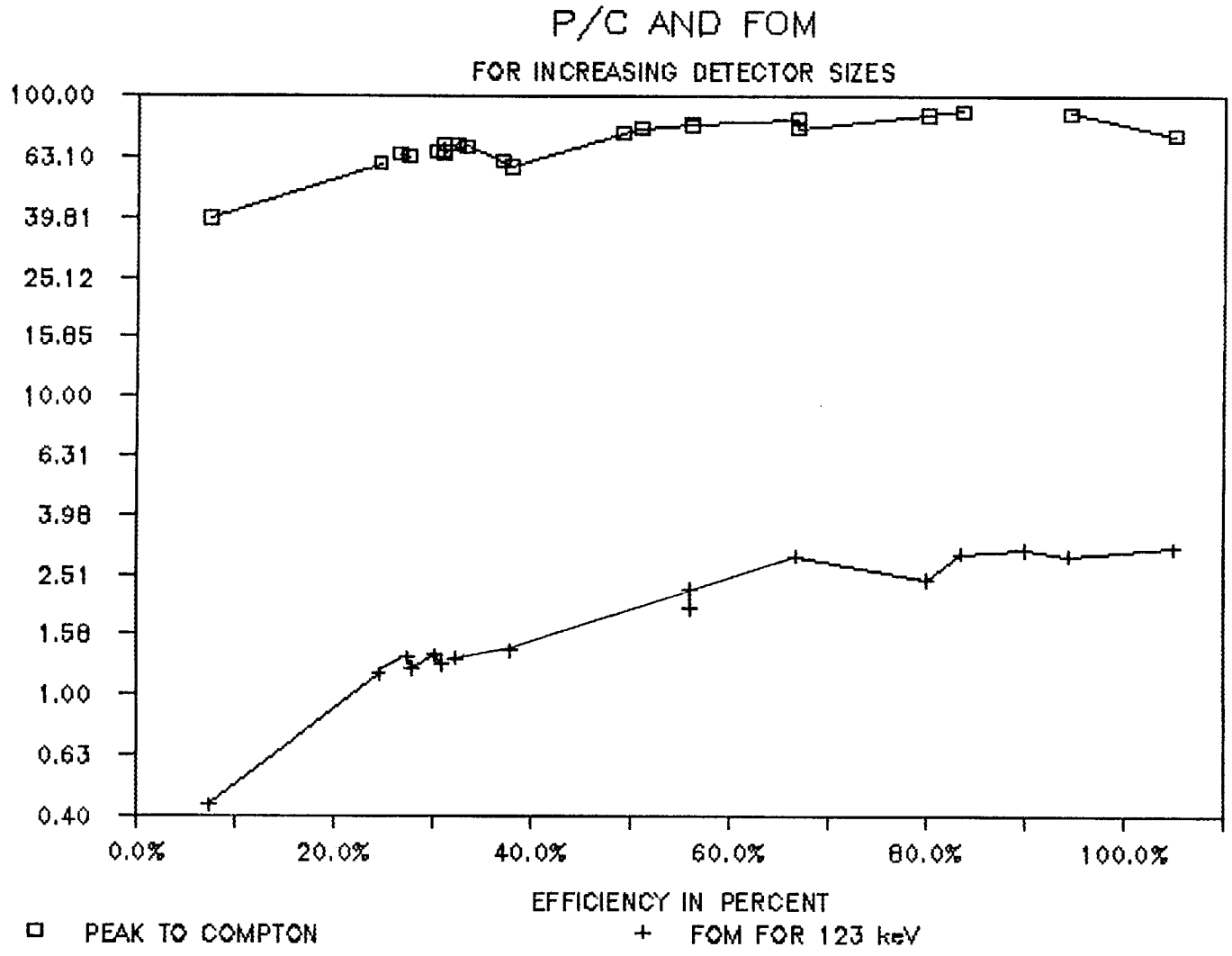

Fig. 25 Comparison of Peak-to-Compton and FOM

if analyzing for the low energy transuranics, a 30% detector with "good" resolution would be a better choice.

7. SUMMARY

The data used in this study were limited to a single manufacturer of high purity germanium detectors. Data acquisition began late in 1986 for the low background detector spectra and ended in mid October of 1989. The standard transplantable detector data acquisition began in mid 1987 and finished in October 1989. The data were graphed as a function of LLD, MDA, and FOM versus energy and relative efficiency. This unique study has acquired a large volume of empirical data from a range of relative efficiency p-type detectors. Sufficient data have been obtained to offer beneficial information for the selection of the most appropriate detector for measuring low levels of radioactivity.

A concise summary of the results is that the detector of choice for low energy photon measurements would be a 25% detector with relatively good resolution, and the detector of choice for photon energies greater than 500 keV would be a large efficiency low background detector. If the entire energy range is of interest, then a 70% low background detector with a high P/C and a resolution of 1.88 keV would yield the lowest MDA and assure the most efficient counting times.

REFERENCES

REFERENCES

1. J.A.Cooper, Nuclear Instruments and Methods, 82, 273-277, (1970).

2. G.F. Knoll, Radiation Detection and Measurement, Second Edition, J. Wiley and Sons, N.Y., 1989.

3. D.C. Camp, C. Gatrousis, L.A. Maynard, Nuclear Instruments and Methods, 117, 189 (1974).

4. R.M. Keyser, G.V. Walford, J.A. Cooper, "Precise Environmental Gamma-Ray Measurements Utilizing Standard Ge(Li) Detectors", Proceedings of 1976 NBS Conference on Nuclear Instrumentation, National Bureau of Standards, SP456, Md., (1976).

5. L.A. Currie, "Lower Limits of Detection: Definition of a Proposed Position for Radiological Effluents and Environmental Measurement", NUREG/CR-4007, Nuclear Regulatory Commission, Batelle, Pacific Northwest Laboratories, PNL, WA, Sept. 1984.

6. J.C. Lochamy, The Minimum Detectable Activity Concept, EG&G ORTEC, PSD No. 17, Oak Ridge, TN., (1981).

7. B.S. Pasternack, N.H. Harley, Nuclear Instruments and Methods 91, 533-540, (1971).

8. OMNIGAM, GammaRay Spectrum Analysis, B30-B1, Software Manual, Software Version, EG&G ORTEC, Oak Ridge, TN., 3.3, 1989.

9. G. Bellia, A. DelZoppo, C. Agodi, R. Alba, R. Coniglione, E. Mignece, G. Russo. and P. Sapienza; Nuclear Instruments and Methods, A284, 399-404, (1989).

APPENDIXES

APPENDIX A

Nuclide and Library Tables

TABLE A.1

Low Background Nuclide Table: Photopeak Energies for Isotopes of Interest in Low Background Studies.

E(keV)	Isotope
46.5	Pb-210
63.3	Th-234 (U)
92.6	Th-234 (U)
185.7	U-235, Ra-226
238.6	Pb-212 (Th)
295.2	Pb-214 (U)
351.9	Pb-214 (U)
511.0	Annihilation Peak
583.1	Bl-214 (U)
609.3	Bi-214 (U)
661.6	Cs-137
727.2	Bi-212 (Th)
766.6	Pa-234m (U)
911.0	Ac-228 (Th)
969.0	Ac-228 (Th)
1001.0	Pa-234m (U)
1120.3	Bi-214 (U)
1173.0	Co-60
1238.0	Bi-214 (U)
1332.5	Co-60
1460.0	K-40
1764.0	Bi-214 (U)
2614.5	Tl-208 (Th)

(U) = U-238 daughters per Ra-226
(Th) = Th-232 series

TABLE A.2
Certificate Table for Mixed Gamma Radionuclide Standard X-Ray and Gamma-Ray Energies, Emission Rates (2.3),and Uncertainties for Standard Reference Material 4275-B

Nuclide	Photon Energy (keV)	Emission Rate (gammas/dis)**	Total Est. Unc. (%)*
^{125}Sb-^{125}Te	K , 27.4	7.977×10^3	1.3
^{154}Eu-^{155}Eu	K , 42.8	5.932×10^3	1.3
^{155}Eu	86.6	3.403×10^3	0.0
^{155}Eu	105.3	2.350×10^3	
^{154}Eu	123.1	8.128×10^3	0.7
^{125}Sb	176.4	8.755×10^3	0.6
^{154}Eu	248.0	1.378×10^3	0.6
^{125}Sb	380.5	1.940×10^3	0.8
^{125}Sb	427.5	3.805×10^3	0.7
^{125}Sb	463.4	1.338×10^3	0.7
^{154}Eu	591.7	9.859×10^3	0.6
^{125}Sb	600.6	2.260×10^3	0.6
^{125}Sb	635.9	1.444×10^3	0.6
^{154}Eu	723.3	4.001×10^3	0.6
^{154}Eu	873.2	2.429×10^3	0.7
^{154}Eu	996.4	2.079×10^3	1.0
^{154}Eu	1004.8	3.604×10^3	0.7
^{154}Eu	1274.4	6.948×10^3	0.6
^{154}Eu	1596.5	3.531×10^2	0.7

*Estimated total uncertainties have the significance of one standard deviation of the mean. Components of these estimates are given in Table III.

**12:00pm EST on May 1, 1983.

TABLE A.3

Activities for Standard Reference Material 4275-B
Serial Number 1417

Nuclide	Becquerels	Microcuries
Eu-154	19772.8	.5344
Eu-155	11011.2	.2976
Sb-125	12883.4	.3482

TABLE A.4

Calibration Library (4275B.LIB). Gamma-ray Energies, Emission Rates, and Half-life Data for SRM -4275b.

Nuclide	E(keV)	Γ/100d	$T_{½}$
Eu-154	123.14	40.50	3130 D
Eu-154	248.04	6.59	3130 D
Eu-154	591.74	4.84	3130 D
Eu-154	723.30	19.70	3130 D
Eu-154	873.19	11.50	3130 D
Eu-154	996.32	10.30	3130 D
Eu-154	1004.76	17.89	3130 D
Eu-154	1274.45	35.50	3130 D
Eu-154	1596.48	1.67	3130 D
Eu-155	86.543	30.80	1741 D
Eu-155	105.308	20.50	1741 D
Sb-125	176.334	6.79	2.73 Y
Sb-125	380.435	1.52	2.73 Y
Sb-125	427.889	29.44	2.73 Y
Sb-125	463.383	10.45	2.73 Y
Sb-125	600.587	17.78	2.73 Y
Sb-125	635.895	11.32	2.73 Y

TABLE A.5

Calibration Library List for Minimum Detectable Activity (MDA) Analysis of SRM 4275b, Filename (4275.LIB), for Peak and Non-Peak Regions of Interest.

Nuclide	E(keV)	Γ/100d	$T_{½}$
Eu-154	1274.45	35.50	3127 D
Eu-154	123.14	40.50	3127 D
Eu-154	723.30	19.70	3127 D
Eu-154	1004.76	17.89	3127 D
Eu-154	873.19	11.50	3127 D
Eu-154	996.32	10.30	3127 D
Eu-154	1596.48	1.67	3127 D
Eu-154	248.04	6.59	3127 D
Eu-154	591.74	4.84	3127 D
Eu-155	86.543	30.80	1741 D
Eu-155	105.308	20.50	1741 D
Sb-125	427.889	29.44	2.73 Y
Sb-125	635.895	11.32	2.73 Y
Sb-125	600.557	17.78	2.73 Y
Sb-125	463.383	10.45	2.73 Y
Sb-125	176.334	6.79	2.73 Y
Sb-125	380.435	1.52	2.73 Y
A-150	150.00	100	500 Y
A-150	275.00	100	500 Y
A-150	525.00	100	500 Y
A-150	780.00	100	500 Y
A-150	1080.00	100	500 Y
A-150	1980.00	100	500 Y
A-150	2250.00	100	500 Y

TABLE A.6

Background Library List for Peak (Pks-100) and Non-Peak (B-150) Regions of Interest for Nuclide Energies, Emission Rates and Half-life.

Nuclide	E(keV)	Γ/100d	$T_{½}$ (Y)
B-150	220.0	100.00	500
B-150	450.0	100.00	500
B-150	700.0	100.00	500
B-150	1400.0	100.00	500
B-150	2300.0	100.00	500
Pks-100	62.5	100.00	500
Pks-100	93.0	100.00	500
Pks-100	238.0	100.00	500
Pks-100	352.0	100.00	500
Pks-100	511.0	100.00	500
Pks-100	583.0	100.00	500
Pks-100	609.0	100.00	500
Pks-100	911.0	100.00	500
Pks-100	1238.0	100.00	500
Pks-100	1764.0	100.00	500
Pks-100	2614.0	100.00	500
K-40	1460.8	10.70	1.28E + 09
Co-60	1173.2	100.00	5.27
Co-60	1332.5	100.00	5.27
Pb-210	46.5	40.00	20.4
Ra-226	185.9	3.28	1600.0

APPENDIX B

Tables for Figures

B.1

RAW DETECTOR DATA

DET #	CRYO	S/N #	% EFF	NUCLIDE ENERGY COUNTTIME	CALIB LIVE TIME	FWHM @ 133keV	PEAK TO COMPTON
1	LB	P20008	40.0%	100000	3600	1.90	65.0
2	LB	P30147	42.6%	100000	3600	1.74	74.2
3	LB	P1784A	44.3%	100000	3600	1.74	76.1
4	LB	P20051	56.5%	100000	3600	1.92	69.8
5	PT	P10125	7.6%	100000	3600	1.66	39.7
6	PT	P10052B	24.6%	100000	3600	1.72	60.1
7	PT	P82M	25.0%	100000	2930		
8	PT	P10364A	26.5%	100000	3600	1.67	64.7
9	PT	P10369A	27.5%	100000	3600	1.67	63.4
10	PT	PK94A	28.0%	100000	3105		
11	PT	P10128	30.3%	100000	3600	1.71	66.2
12	PT	P30323B	31.0%	100000	3600	1.65	70.0
13	PT	P20237	31.0%	100000	3600	1.70	65.5
14	PT	P10328	32.3%	100000	3600	1.67	69.9
15	PT	P10113	31.0%	100000		1.71	66.1
16	PT	P10063	33.3%	100000		1.73	68.6
17	PT	P30140	37.0%	100000	1770	2.00	61.3
18	PT	P30036A	38.0%	100000	2900	2.05	59.1
19	PT	P30183	49.0%	100000	2180	1.72	75.9
20	PT	P30164A	51.0%	100000	6587	1.73	79.1
21	PT	P30165	56.0%	100000	3480	1.76	81.1
22	PT	P30158	56.0%	100000	3594	1.79	81.3
23	PT	P40045	66.6%	100000	3600	1.84	85.0
24	PT	P30195	66.7%	100000	3600	1.88	78.9
25	PT	P20085	80.0%	100000	3600	1.83	87.1
26	PT	P20149	83.3%	100000	3600	1.86	89.8
27	PT	P20160	89.9%	100000	3600		
28	PT	P20155	94.3%	100000	3609	1.97	88.1
29	PT	P20239A	104.9%	100000	3600	2.36	74.8

B.2

FIGURE OF MERIT AT 123 keV FOR SELECTED DETECTORS
TO PLOT FIGURES 6 AND 9

DET #	%EFF	123 FWHM	LIVE TIME	123 GROSS	123 NET	123 %EFF	123 FOM
1	40.0%	1.051	3600	263498	224149	0.010000	1.934931
2	42.6%	1.052	3600	242339	221851	0.011000	1.535092
3	44.3%	1.016	3600	279753	258522	0.010000	1.445567
4	56.5%	1.051	3600	308955	288790	0.010000	1.385153
5	7.6%	1.240	3600	102970	94230	0.005125	0.430267
6	24.6%	1.090	3600	206268	190642	0.009790	1.172177
9	27.5%	0.998	3600	200058	184759	0.010800	1.337180
10	28.0%	1.060	3105	181717	169324	0.010520	1.224817
11	30.3%	0.974	3600	214244	199000	0.010810	1.350595
12	31.0%	1.300	3600	206133	187219	0.010600	1.278574
14	32.3%	1.190	3600	214138	197435	0.011200	1.326910
18	38.0%	1.005	2901	174031	160031	0.010670	1.402887
21	56.0%	0.982	3480	293064	271902	0.015200	2.269487
22	56.0%	1.220	3594	275401	250148	0.013440	1.935254
24	66.7%	0.999	3600	359040	334279	0.018280	2.877912
25	80.0%	1.180	3600	311207	285266	0.016300	2.416795
26	83.3%	1.100	3600	325784	299026	0.018900	2.947761
27	89.9%	1.250	3600	380680	349417	0.019250	3.044325
28	94.3%	1.770	3609	404458	366783	0.019870	2.895314
29	104.9%	1.464	3600	378128	341154	0.018930	3.008349

B.3

FIGURE OF MERIT AT 1274 keV FOR SELECTED DETECTORS
TO PLOT FIGURES 6 AND 9

DET #	%EFF	1274 FWHM	LIVE TIME	1274 GROSS	1274 NET	1274 %EFF	1274 FOM
1	40.0%	1.889	3600	42189	41509	0.002000	0.037946
2	42.6%	1.848	3600	43670	42931	0.002000	0.039994
3	44.3%	1.956	3600	50027	48939	0.002000	0.047169
4	56.5%	1.945	3600	56030	54989	0.002000	0.046269
5	7.6%	1.950	3600	8256	8193	0.000495	0.002811
6	24.6%	1.990	3600	26769	26398	0.001519	0.020740
9	27.5%	1.890	3600	28841	28190	0.001900	0.035262
10	28.0%	2.200	3105	27076	26776	0.001898	0.023865
11	30.3%	1.820	3600	31776	31530	0.001920	0.022321
12	31.0%	2.000	3600	29936	29361	0.001900	0.032216
14	32.3%	1.970	3600	32759	32228	0.002100	0.034477
18	38.0%	2.110	2901	29248	28819	0.002140	0.033992
21	56.0%	1.900	3480	53920	53015	0.003360	0.074584
22	56.0%	1.940	3594	54598	53593	0.003264	0.074352
24	66.7%	1.880	3600	65794	64518	0.003973	0.103505
25	80.0%	1.890	3600	70090	69166	0.004740	0.104805
26	83.3%	1.950	3600	76667	76089	0.004500	0.077474
27	89.9%	2.080	3600	84075	82681	0.005045	0.130605
28	94.3%	2.570	3609	88423	86861	0.005374	0.132321
29	104.9%	2.453	3600	94700	92719	0.005834	0.165790

B.4

LOWER LIMITS OF DETECTION AT BACKGROUND PEAK ENERGIES
FOR FIGURES 7, 10, 11, AND 12.

DET #	S/N #	% EFF	92 (keV)	238 (keV)	583 (keV)	1460 (keV)	2614 (keV)
5	P10125	7.6%	0.441	0.569	0.625	1.057	0.000
6	P10052B	24.6%	0.265	0.319	0.358	0.585	0.727
7	P82M	25.0%	0.341	0.385	0.425	0.657	0.778
10	PK94A	28.0%	0.248	0.266	0.304	0.518	0.561
11	P10128	30.3%	0.247	0.294	0.327	0.505	0.592
17	P30140	37.0%	0.262	0.294	0.312	0.477	0.552
18	P30036	38.0%	0.284	0.299	0.366	0.701	0.839
19	P30183	49.0%	0.208	0.271	0.283	0.397	0.528
20	P30164A	51.0%	0.205	0.268	0.272	0.392	0.428
21	P30165	56.0%	0.224	0.268	0.280	0.539	0.548
22	P30158	56.0%	0.228	0.288	0.284	0.457	0.513
24	P30195	66.7%	0.183	0.222	0.245	0.341	0.415
26	P20149	83.3%	0.300	0.326	0.301	0.414	0.419
27	P20160	89.9%	0.201	0.258	0.250	0.410	0.460
29	P20239A	104.9%	0.249	0.271	0.284	0.600	0.481
1	P20008	40.0%	0.173	0.211	0.222	0.334	0.391
2	P30147	42.6%	0.141	0.000	0.227	0.339	0.367
3	P1784A	44.3%	0.176	0.234	0.228	0.480	0.425
4	P20051	56.5%	0.202	0.180	0.195	0.413	0.362

B.5

CALIBRATION SPECTRA MINIMUM DETECTABLE ACTIVITIES (MDA) AT NON-PEAK ENERGIES (A-150) FOR FIGURES 13 AND 16.

DET #	S/N #	%EFF	MDA VALUES IN BECQUERELS 150 (keV)	275 (keV)	525 (keV)	780 (keV)
5	P10125	8.0%	3.5312	5.3335	8.7274	11.136
6	P10052B	25.0%	2.1414	3.3014	4.8315	5.9052
8	P10364A	27.0%	2.3008	2.8781	4.8448	5.2678
9	P10369A	28.0%	1.9469	2.5446	4.2415	5.0866
11	P10128	30.0%	1.9391	2.4922	4.1261	4.545
14	P10328	32.0%	2.3129	2.9472	4.4821	4.8357
13	P20237	37.0%	2.0138	2.5982	4.194	5.0395
21	P30165	56.0%	1.7196	1.9886	2.989	3.6651
22	P30158	56.0%	2.2058	2.5397	3.1904	3.7872
25	P20085	60.0%	1.7669	2.1407	2.6602	2.9751
26	P20149	83.0%	1.8543	2.238	2.7391	3.1155
27	P20160	90.0%	2.507	2.7966	3.6002	4.2834
28	P20155	94.0%	2.0788	2.415	2.9414	3.2741

CALIBRATION SPECTRA - A150 (CONTINUED)

DET #	S/N #	%EFF	MDA VALUES IN BECQUERELS 1080 (keV)	1980 (keV)	2250 (keV)
5	P10125	8.0%	10.494	2.7579	3.8409
6	P10052B	25.0%	5.4447	1.1973	1.2862
8	P10364A	27.0%	4.9986	1.1999	1.6188
9	P10369A	28.0%	4.1977	1.222	1.0803
11	P10128	30.0%	4.2254	1.0411	1.0406
14	P10328	32.0%	4.4466	1.0501	0.87415
13	P20237	37.0%	4.5814	1.088	1.2474
21	P30165	56.0%	3.1182	0.9342	0.91162
22	P30158	56.0%	3.0974	0.96766	0.88493
25	P20085	60.0%	2.5941	0.52905	0.48482
26	P20149	83.0%	2.58	0.68911	0.79996
27	P20160	90.0%	3.6125	0.92119	0.96788
28	P20155	94.0%	2.7285	0.65056	0.71524

B.6

BACKGROUND SPECTRA MINIMUM DETECTABLE ACTIVITIES (MDA)
AT NON-PEAK ENERGIES (B150) FOR FIGURES 14 AND 17

MDA VALUES IN BECQUERELS

DET #	S/N #	%EFF	220 (keV)	450 (keV)	700 (keV)	1400 (keV)	2300 (keV)
6	P10052BB	25.0%	0.0454	0.0568	0.0692	0.0595	0.0783
11	P10128BK	30.0%	0.0424	0.0505	0.0521	0.0544	0.0599
14	P103288BK	32.0%	0.0505	0.0505	0.0621	0.0527	0.0547
13	P20237BK	37.0%	0.0508	0.0517	0.0600	0.0531	0.0555
24	P30195BK	67.0%	0.0320	0.0362	0.0391	0.0351	0.0372
26	P20149BK	83.3%	0.0495	0.0457	0.0521	0.0436	0.0448
29	P20239AB	105.0%	0.0509	0.0447	0.0503	0.0410	0.0350

B.7

BACKGROUND SPECTRA MINIMUM DETECTABLE ACTIVITIES (MDA)
AT PEAK ENERGIES (PKS-100) FOR FIGURE 15

			MDA IN BECQUERELS				
DET #	S/N #	%EFF	62 (keV)	93 (keV)	238 (keV)	352 (keV)	511 (keV)
6	P10052BB	25.0%	0.0605	0.0569	0.0656	0.0605	0.1009
9	P10369AB	28.0%	0.0596	0.0525	0.0570	0.0478	0.0932
11	P10128BK	30.3%	0.0598	0.0519	0.0608	0.0481	0.0951
13	P20237BK	37.0%	0.0608	0.0566	0.0691	0.0560	0.0917
17	P30140BK	37.0%	0.0564	0.0518	0.0588	0.0540	0.0908
19	P30183BK	49.0%	0.0444	0.0426	0.0547	0.0411	0.0689
25	P20085B1	80.0%	0.0631	0.0467	0.0480	0.0397	0.0616
29	P20239AB	105.0%	0.0449	0.0524	0.0636	0.0518	0.0715

PEAKS 100 (CONTINUED)

		MDA IN BECQUERELS					
DET #	%EFF	583 (keV)	609 (keV)	911 (keV)	1238 (keV)	1764 (keV)	2614 (keV)
6	25.0%	0.0777	0.0825	0.0764	0.0724	0.0775	0.1180
9	28.0%	0.0659	0.0629	0.0642	0.0557	0.0733	0.1383
11	30.3%	0.0726	0.0685	0.0638	0.0528	0.0718	0.1324
13	37.0%	0.0690	0.0671	0.0642	0.0566	0.0554	0.0631
17	37.0%	0.0667	0.0629	0.0626	0.0591	0.0709	0.1254
19	49.0%	0.0554	0.0442	0.0452	0.0425	0.0547	0.1221
25	80.0%	0.0451	0.0426	0.0398	0.0351	0.0433	0.0672
29	105.0%	0.0630	0.0610	0.0522	0.0490	0.0578	0.1090

B.8

BACKGROUND SPECTRA LOWER LIMIT OF DETECTION (LLD)
FOR DIFFERENT COUNT TIMES AT PEAK ENERGIES
TO PLOT FIGURE 19

DET #	COUNT TIME (SEC)	PLLD	ABS EFF	LLD
			93keV	
P20149	10000	4.40E-02	0.0147	3.0015
	20000	2.20E-02	0.0147	1.5007
	60000	7.33E-03	0.0147	0.5002
	80000	5.50E-03	0.0147	0.3752
	100000	4.40E-03	0.0147	0.3001
			1461 keV	
	10000	1.73E-02	0.0042	4.1394
	20000	8.65E-03	0.0042	2.0697
	60000	2.88E-03	0.0042	0.6899
	80000	2.16E-03	0.0042	0.5174
	100000	1.73E-03	0.0042	0.4139

B.9

COUNT TIME VERSUS MINIMUM DETECTABLE ACTIVITY (MDA)
FOR FIGURES 20, 21, 22, 23 AND 24.

			MDA VALUES IN BECQUERELS				
DET #	%EFF	COUNT TIME (SEC)	220 (keV)	450 (keV)	700 (keV)	1400 (keV)	2300 (keV)
26	83.3%	10000	0.1667	0.1361	0.1620	0.1298	0.1540
		20000	0.1134	0.0975	0.1175	0.0918	0.1089
		60000	0.0643	0.0592	0.0674	0.0557	0.0570
		80000	0.0550	0.0512	0.0580	0.0484	0.0499
		100000	0.0495	0.0457	0.0521	0.0436	0.0448
6	25.0%	10000	0.1527	0.1693	0.2153	0.1772	0.2690
		20000	0.1038	0.1212	0.1562	0.1253	0.1902
		60000	0.0589	0.0737	0.0896	0.0761	0.0996
		80000	0.0504	0.0637	0.0771	0.0661	0.0873
		100000	0.0454	0.0568	0.0692	0.0595	0.0783
17	37.0%	10000	0.1075	0.1079	0.1216	0.1045	0.1279
		20000	0.0731	0.0772	0.0882	0.0739	0.0904
		60000	0.0415	0.0469	0.0506	0.0449	0.0473
		80000	0.0355	0.0406	0.0436	0.0390	0.0415
		100000	0.0320	0.0362	0.0391	0.0351	0.0372

B.10

COUNT TIME VERSUS FIGURE OF MERIT (FOM) 1/MDA FOR FIGURE 21

DET #	%EFF	COUNT TIME (SEC)	220 (keV)	450 (keV)	700 (keV)	1400 (keV)	2300 (keV)
26	83.3%	10000	5.9981	7.3454	6.1725	7.7065	6.4939
		20000	8.8215	10.2617	8.5106	10.8989	9.1836
		60000	15.5594	16.8862	14.8326	17.9498	17.5423
		80000	18.1663	19.5126	17.2354	20.6560	20.0208
		100000	20.1857	21.8924	19.2090	22.9537	22.3179

B.11

PEAK-TO-COMPTON (P/C) AND FIGURE OF MERIT (FOM)
VALUES TO PLOT FIGURE 25

DET #	S/N #	% EFF	NUCLIDE ENERGY COUNTTIME	CALIB LIVE TIME	FWHM @ 133keV	PEAK TO COMPTON	123 (keV) FOM
1	P20008	40.0%	100000	3600	1.90	65.0	1.93
2	P30147	42.6%	100000	3600	1.74	74.2	1.53
3	P1784A	44.3%	100000	3600	1.74	76.1	1.44
4	P20051	56.5%	100000	3600	1.92	69.8	1.38
5	P10125	7.6%	100000	3600	1.66	39.7	0.43
6	P10052B	24.6%	100000	3600	1.72	60.1	1.17
7	P82M	25.0%	100000				
8	P10364A	26.5%	100000		1.67	64.7	
9	P10369A	27.5%	100000	3600	1.67	63.4	1.33
10	PK94A	28.0%	100000	3105			1.22
11	P10128	30.3%	100000	3600	1.71	66.2	1.35
12	P30323B	31.0%	100000	3600	1.65	70.0	1.27
13	P20237	31.0%	100000		1.70	65.5	
14	P10328	32.3%	100000	3600	1.67	69.9	1.32
15	P10113	31.0%	100000		1.71	66.1	
16	P10063	33.3%	100000		1.73	68.6	
17	P30140	37.0%	100000		2.00	61.3	
18	P30036A	38.0%	100000	2901	2.05	59.1	1.4
19	P30183	49.0%	100000	2188	1.72	75.9	
20	P30164A	51.0%	100000	6587	1.73	79.1	
21	P30165	56.0%	100000	3480	1.76	81.1	2.26
22	P30158	56.0%	100000	3594	1.79	81.3	1.93
23	P40045	66.6%	100000		1.84	85.0	
24	P30195	66.7%	100000	3600	1.88	78.9	2.89
25	P20085	80.0%	100000	3600	1.83	87.1	2.41
26	P20149	83.3%	100000	3600	1.86	89.8	2.94
27	P20160	89.9%	100000	3600			3.04
28	P20155	94.3%	100000	3609	1.97	88.1	2.89
29	P20239A	104.9%	100000	3600	2.36	74.8	3.08

INTERNAL DISTRIBUTION

1-2. Central Research Library
3. Document Reference Section
4-5. Laboratory Records Department
6. Laboratory Records, ORNL RC
7. ORNL Patent Section
8. Bogard, J. S.
9. Bryan, W. L.
10-35. Buker, L. M.
36. Burchfield, L. A.
37. Childs, M. R.
38. Duncan, D. T.
39. Forbes, R. J.
40. Halliburton, R. E.
41. Hunt, J. B.
42. Larsen, I. L.
43. Mlekodaj, R. L.
44. Rao, G. R.
45. Row, T. H.
46. Setaro, J. A.
47. Swanks, J. H.
48. Thein, M.

EXTERNAL DISTRIBUTION

49. A. C. Bassett, DOE/ORO

50. L. F. Miller, Department of Nuclear Engineering
University of Tennessee
Knoxville, TN 37996-2300

51. Office of Assistant Manager for Energy Research and Development,

52-53. Office of Scientific and Technical Information, P. O. Box 62, Oak Ridge, TN 37830